

Response to Comments on “Diel variation of mercury stable isotope ratios record photoreduction of PM_{2.5}-bound mercury”

Qiang Huang^{1*}, Weilin Huang², John R. Reinfeld²

¹ State Key Laboratory of Environmental Geochemistry, Institute of Geochemistry, CAS, Guiyang 550081, China

² Department of Environmental Sciences, Rutgers, The State University of New Jersey, New Brunswick, NJ 08901, USA

*Corresponding author.

E-mail: huangqiang@vip.gyig.ac.cn

We thank the reviewers for their constructive comments and suggestions. We have completed the revision of the manuscript according to the comments and suggestions provided by the reviewers. We appreciate very much all comments made by the reviewers; they are very valuable for improving the readability of the manuscript and interpretation of the protocol. Detailed Response, Marked Manuscript and Revised Supporting Information were also combined into a PDF file in supplement. In the marked version, the revised areas are in red color. Please check the file in supplement. Below we have compiled our point-by-point responses to the comments.

Detailed Responses to Referees

1 Anonymous Referee #1

Received and published: 11 October 2018

Huang et al. present a study on diurnal particulate (aerosol) Hg isotope variation in Beijing. I have reviewed this MS previously for ES&T and I was curious to see how the MS evolved following my previous suggestions. I regret to say that these have been largely ignored, so I paste here my previous review because it is still of interest: “Huang et al.’s study is unique and the variations observed, with lower Hg concentrations and higher Hg MIF during daytime, are rather interesting and novel. The authors interpret this as evidence for in-aerosol photoreduction of Hg, which would be an important result if it were true. The MS is fairly well written, organized and cited.

--Thank you for your comments. We have addressed the comments below.

Although at first sight I agree with the interpretation, I find that the authors privilege the photoreduction interpretation without much in-depth discussion of alternative interpretations. For example, the current gas-aerosol partitioning model (Amos et al., 2012, ACP) suggests divalent gaseous Hg (GOM) to partition to aerosol at low temperatures. The authors should estimate and discuss if this process can lead to their concentration observations.

--Thanks for the above comments. In this study, we observed that PBM (mass-based concentration) is greater during night-time than daytime for consecutive day-night pairs. We agree with the reviewer that the PBM is likely affected by gas-aerosol partitioning of GOM, in addition to the impact of sources. It is intuitive that the partitioning equilibrium depends on both temperature and GOM level. Adsorption or partitioning of GOM from air to PM is an exothermic process; lower temperature at night-time favors stronger adsorption of GOM on PM than at day-time.

For example, Rutter and Schauer (2007) and Amos et al. (2012) proposed gas-aerosol partitioning models, which suggest that more divalent gaseous Hg (GOM) may partition onto aerosols at lower temperature. If we assume that GOM could remain a constant level during daytime and night-time, relatively lower temperature at night-time should result in higher PBM in the night-time than in the daytime. However, the assumption of constant GOM over day-night time is likely untrue. According to several recent studies, the GOM measured in the field also exhibits significant diel variation, with higher GOM concentrations found during the daytime than at night (Poissant et al., 2005; Liu et al., 2007; Lan et al., 2012), likely due to the photo-oxidation of GEM. For example, the GOM measured during the spring season in Salt Lake city was equal to or lower than 4 pg m^{-3} at night-time and was as high as 20 pg m^{-3} during daytime (Lan et al., 2012). Another study reported that the GOM measured in the urban area of Detroit, Michigan was lower than 9 pg m^{-3} at night and as high as 13 pg m^{-3} during day-time (Liu et al., 2007). Apparently, the temperature effect on PBM concentration due to favored adsorption of GOM during night-time (lower temperature) may be partially (if not totally) offset by lower GOM levels during night-time. In other words, the net PBM may show less diel variation as predicted from the temperature-dependent partitioning model when GOM is also substantially lowered during the night-time.

To support the above argument, we used an inverse approach and a GOM partitioning model to compute hypothetical GOM levels corresponding to each of our PBM observations at ambient temperature. We used the GOM gas-aerosol partitioning model proposed by Amos et al., 2012, which has the following equation: $\log_{10}(K^{-1}) = (10 \pm 1) - (2500 \pm 300)/T$, where $K = (\text{PBM}/\text{PM}_{2.5})/\text{GOM}$ with PBM and GOM in common volumetric units (pg m^{-3}), $\text{PM}_{2.5}$ in $\mu\text{g m}^{-3}$, and T in K. We used the measured $\text{PM}_{2.5}\text{-Hg}$ as PBM and assumed that the $\text{PM}_{2.5}\text{-Hg}$ measured for each sample is 100% in divalent and active mercury forms. The calculated GOM concentrations are presented in the following Table R1. In summary, the calculated GOM

concentrations range from 1.5 to 31 pg m^{-3} , with average values of $11\pm 5 \text{ pg m}^{-3}$ during the daytime and $13\pm 7 \text{ pg m}^{-3}$ during the nighttime. Overall, the calculated GOM exhibit insignificant ($p = 0.195$, paired samples t -test) diel variation of GOM concentration, i.e., there would be little or no difference of GOM between day- and night-time. Close inspection of the data (Table R1) showed that half of the paired day-night samples have higher calculated GOM concentrations during the nighttime than in daytime. This is opposite to the prior findings cited above (Poissant et al., 2005; Liu et al., 2007; Lan et al., 2012) showing higher measured GOM in the daytime than in the nighttime and indicates that processes other than gas-aerosol partitioning control GOM concentrations in the environment.

Similarly, gas-aerosol partitioning of GOM does not likely account for the diel variation of $\text{PM}_{2.5}\text{-Hg}$ concentrations measured in this study.

Table R1. Calculated GOM concentrations of day and night samples. The value of GOM concentrations higher at night than the consecutively days are in bold text.

Daytime samples	Ave. T (°C)	Hg Con. ($\mu\text{g g}^{-1}$)	K ($\text{m}^3 \mu\text{g}^{-1}$)	GOM (pg m^{-3})	Nighttime samples	Ave. T (°C)	Hg Con. ($\mu\text{g g}^{-1}$)	K ($\text{m}^3 \mu\text{g}^{-1}$)	GOM (pg m^{-3})
Sept-16-D	24.1	0.41	0.026	16	Sept-15-N	19.8	0.52	0.035	15
Sept-17-D	24.8	0.38	0.025	15	Sept-16-N	21.1	0.44	0.032	14
Sept-18-D	27.3	0.17	0.021	8.0	Sept-17-N	22.6	0.47	0.029	16
Sept-19-D	26.1	0.09	0.023	3.9	Sept-18-N	21.7	0.31	0.030	10
Sept-20-D	24.5	0.61	0.025	24	Sept-19-N	21.7	0.29	0.030	10
Sept-21-D	25.2	0.48	0.024	20	Sept-20-N	21.9	0.89	0.030	30
Sept-22-D	22.9	0.53	0.028	19	Sept-21-N	22.6	0.62	0.029	22
Sept-23-D	23.9	0.15	0.026	5.7	Sept-22-N	18.3	0.31	0.038	8.1
Sept-24-D	23	0.38	0.028	14	Sept-23-N	21.6	0.54	0.031	18
Sept-25-D	24.4	0.38	0.025	15	Sept-24-N	17.7	0.2	0.040	5.0
Sept-26-D	23.7	0.2	0.027	7.5	Sept-25-N	17.3	0.14	0.041	3.4
Sept-27-D	23.8	0.39	0.026	15	Sept-26-N	20.5	0.44	0.033	13
Sept-28-D	18.1	0.32	0.039	8	Sept-27-N	-	0.78		
Sept-29-D	15.7	0.48	0.046	11	Sept-28-N	17.4	0.34	0.041	8.4
Sept-30-D	18.1	0.16	0.039	4.1	Sept-29-N	14.7	0.36	0.049	7.4
Oct-1-D	19.4	0.12	0.035	3.4	Sept-30-N	15.5	0.64	0.046	14
Oct-2-D	24.3	0.2	0.026	7.8	Oct-1-N	15.8	0.67	0.045	15
Oct-3-D	22.5	0.26	0.029	9.0	Oct-2-N	18.4	0.59	0.038	16
Oct-4-D	21.5	0.36	0.031	12	Oct-3-N	17.7	0.59	0.040	15
Oct-5-D	21.8	0.37	0.030	12	Oct-4-N	17.9	0.38	0.039	10
Oct-6-D	23	0.39	0.028	14	Oct-5-N	18.3	0.53	0.038	14
Oct-7-D	22.6	0.47	0.029	16	Oct-6-N	19.8	0.44	0.035	13
Oct-8-D	17.8	0.3	0.040	7.6	Oct-7-N	19.1	0.46	0.036	13
					Oct-8-N	14.3	0.24	0.050	4.8

Oct-9-D	18.7	0.43	0.037	12	Oct-9-N	12.5	0.08	0.057	1.4
Oct-10-D	14.4	0.19	0.050	3.8	Oct-10-N	15.3	0.26	0.047	5.5
Oct-11-D	20.1	0.1	0.034	3.0	Oct-11-N	16.6	0.38	0.043	8.9
Oct-12-D	22.5	0.27	0.029	9.4	Oct-12-N	17.8	1.22	0.040	31
Oct-13-D	23.7	0.43	0.027	16	Oct-13-N	17.2	0.89	0.041	22
Oct-14-D	20.1	0.37	0.034	11	Oct-14-N	16.3	0.49	0.044	11
Oct-15-D	22.5	0.34	0.029	12	Oct-15-N	19.7	0.33	0.035	9.5

Meanwhile, our data showed that the average $\Delta^{199}\text{Hg}$ value during the daytime ($0.26\text{‰} \pm 0.40\text{‰}$, 1SD, $n = 26$) is (statistically) significantly ($p < 0.05$, t-test) higher than during the nighttime ($0.04\text{‰} \pm 0.22\text{‰}$, 1SD, $n = 30$). This slight diel variation of odd-MIF of Hg isotopes was explained in terms of photoreduction of PBM during daytime. In addition we argue that the diel variations of odd-MIF of Hg isotopes does not result from GOM gas-aerosol partitioning. In general, divalent Hg gas-aerosol partitioning is considered as chemisorption and desorption (Rutter and Schauer, 2007). Prior studies showed that the adsorption/desorption and precipitation of aqueous Hg^{2+} had insignificant odd-MIF of Hg isotopes (Jiskra et al., 2012; Smith et al., 2015), suggesting that the GOM partitioning process may not result in the characteristics of odd-MIF of Hg isotopes we observed for the $\text{PM}_{2.5}$ samples.

In conclusion, gas-particle partitioning may increase PBM during the night-time due to relatively lower temperature compared to the daytime. The actual increase of PBM during the nighttime may be off-set by lower GOM levels during nighttime when little or no production of GOM by the photo-oxidation of GEM may occur. It is shown that GOM is high during daytime likely due to stronger photo-oxidation. GOM can be adsorbed on to PM where the active Hg species are also photo-reduced to elemental mercury. Such a dynamic and complex adsorption-photoreduction cycle yields lowered PBM levels, along with characteristic Hg isotope properties. In other words, our thesis is that the photochemical reactions cause the concentration reduction of $\text{PM}_{2.5}\text{-Hg}$ as well as fractionation of the $\text{PM}_{2.5}$ -bound Hg isotope compositions.

To address these issues, we have included a discussion about the possible effects of gas-aerosol partitioning on the diel variation of PBM. See the revised manuscript on line 358 to

370, it reads: “A possible explanation of the observed effects of diel variation of PM_{2.5}-Hg would be the temperature-dependent gas-aerosol partitioning of GOM (Rutter and Schauer, 2007; Amos et al., 2012), which favors more adsorption of GOM on PM during nighttime when atmospheric temperature is relatively lower than daytime. However, the magnitude of such adsorption is also proportional to the GOM concentration in the atmosphere. An inverse calculation exercise (in SI) shows that the higher PM_{2.5}-Hg measured for our samples would require higher GOM concentrations during the nighttime, which contradicts with prior findings that GOM concentrations are significantly lower during the nighttime than the daytime as GOM is a product of photo-oxidation processes (Poissant et al., 2005; Liu et al., 2007; Amos et al., 2012). In addition, GOM gas-aerosol partitioning is considered a chemisorption and desorption process (Rutter and Schauer, 2007), which unlikely result in appreciable odd-MIF of Hg isotopes (Jiskra et al., 2012; Smith et al., 2015). Therefore, GOM partitioning would have little or no effect on the observed diel variations of $\Delta^{199}\text{Hg}$ values for PM_{2.5}-Hg.”

I suggest the authors consider the influence of boundary layer dynamics and stratification: daytime turbulence could lead to mixing of above lying, cleaner free tropospheric air with high MIF, whereas nighttime stratification traps Hg emissions with low MIF.”

--Thank you for your suggestion. We agree that the boundary layer was higher during the daytime than at night, and daytime turbulence could help to mix the air between bottom and top of the layer. As you suggest, with constant Hg emission and PM_{2.5} deposition rates, Hg²⁺ photoreduction on PM_{2.5} during the daytime may be enhanced at the top of the boundary layer (up to 1500 m) on a sunny day and produce much more positive odd-MIF of Hg isotopes on PM_{2.5}, while at night, the lower boundary layer traps a portion of daytime PBM at much low altitudes (mean of about 300 m). The mixing of residual daytime PBM with newly emitted

PBM in the thinner boundary layer at night may help to explain why nighttime PBM had odd-MIF values closer to source emissions.

Per your suggestions and comments, we have added a discussion about the possible effects of the difference of boundary layer thickness during daytime and nighttime on the diel variations of Hg isotope ratios in the PM_{2.5} samples we collected. See the revised manuscript on line 371 to 381, it reads: “Variation in atmosphere boundary layer height (ABLH) from 1000 to 1300 m during daytime to less than 200 to 300 m during nighttime may have contributed to the diel variation in Hg isotopic composition of PM_{2.5}-Hg (Quan et al., 2013). With a high ABLH during daytime, relatively strong turbulence may help mixing the PM_{2.5}-Hg from the surface to the upper free troposphere, where photoreactions may be favored due to higher intensities of ultraviolet radiation on clear days. In contrast, a lower ABLH at night may weaken the vertical transport of PM_{2.5}-Hg, but enhance the contribution from newly produced PM_{2.5}-Hg, possibly resulting in higher concentrations of PM_{2.5}-Hg with negative or close to zero $\Delta^{199}\text{Hg}$ values from emission sources and/or GOM. However, vertically-resolved, day-night measurements of Hg stable isotope ratios in PBM and GOM are needed to fully evaluate the effects of various physical processes on diel variation of the Hg isotopic compositions for the PM_{2.5}”.

In the current MS submitted to ACP I did not find discussion of gaseous Hg(0) – aerosol partitioning, nor discussion of boundary layer dynamics. The authors should discuss with atmospheric physicists, and see if proxies of boundary layer mixing can be used. For ex. PM_{2.5} itself seems higher during nighttime than daytime, which is likely due to nighttime boundary layer stratification which traps pollutant emissions. Daytime heating of land and ensuing turbulence will mix boundary layer air with overlying free tropospheric air. Such mixing may, or may not, generate all the trends observed. It should be discussed and counter-argued.

--We agree that, although PM_{2.5} concentrations had insignificant diel variation ($p = 0.887$, paired samples t -test), the change of boundary layer thickness between daytime and nighttime could affect PBM transformations, and we now address the possibility of this effect as described in our comments above.

In summary, I am convinced that the dataset is novel and of strong interest to the atmospheric Hg community and ACP readers, but I suggest the authors to better think through alternative interpretations, and to respect the reviewing process. The editor and reviewers spend time to try and make your study better.

--Thank you for your suggestions and comments. Although the editor of ES&T did not give us a chance to respond to your comments, we truly appreciate the editor and reviewers for their comments on this manuscript. We are very glad to have this chance to respond to your comments at here, and we revised the manuscript accordingly.

Minor comments:

L99. "It is intuitive that, while both D and N PM_{2.5} samples may have similar local or regional sources if the wind trajectory remains unchanged, D samples could have been exposed to more solar radiation than N samples, likely resulting in diel variations in the Hg isotope compositions that are indicative of differences in photochemical transformation of PM_{2.5}-Hg." Not sure this makes sense: if PM-Hg was emitted 1 week ago and travelled across China, the particles went through 7 day/night periods, all receiving more or less the same amount of radiation.

--We have deleted this sentence.

L211. The statistics of diel variations are discussed here, with reference to Table S3. It appears to me that paired T-tests should be reported in the text, and not means and p values for the whole dataset. A key question is whether PM_{2.5} shows diel variation in the paired T-test? The p values in the text do not correspond to metrics in Table S3, so the discussion is hard to follow.

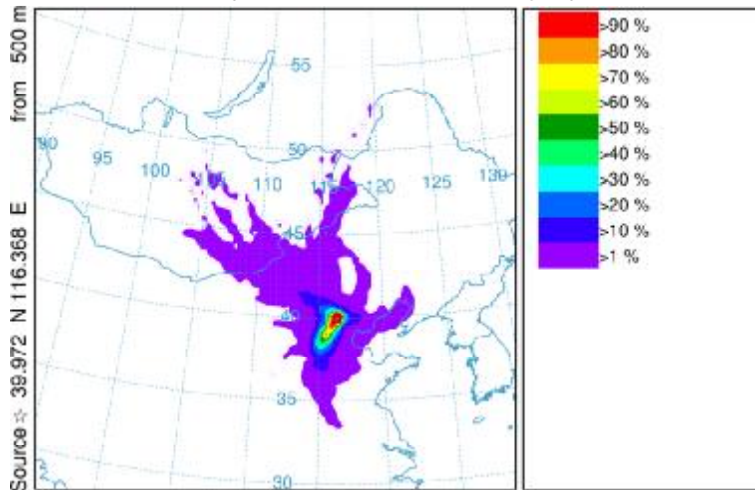
--We have revised this paragraph per your suggestions, which now reads (on line 207 to 215 in the revised manuscript): “T-test results (Table S3) showed that diel variation was statistically significant ($p < 0.05$) for Hg contents, $\Delta^{199}\text{Hg}$, and $\Delta^{200}\text{Hg}$ values, as their p values are 0.005, 0.000 and 0.004 resulting from paired samples t -test, and are 0.003, 0.017 and 0.019 resulting from independent samples t -test. For all samples, Hg contents for D-samples ($0.32 \pm 0.14 \mu\text{g g}^{-1}$) were lower than N-samples ($0.48 \pm 0.24 \mu\text{g g}^{-1}$), and $\Delta^{199}\text{Hg}$ and $\Delta^{200}\text{Hg}$ values for D-samples (mean of $0.26\text{‰} \pm 0.40\text{‰}$ and $0.09\text{‰} \pm 0.06\text{‰}$, respectively) were higher than N-samples ($-0.04\text{‰} \pm 0.22\text{‰}$ and $0.06\text{‰} \pm 0.05\text{‰}$, respectively). However, PM_{2.5} concentrations and $\delta^{202}\text{Hg}$ had statistically insignificant ($p > 0.05$) diel variation, as their p values are 0.887 and 0.052 resulting from paired samples t -test, and are 0.909 and 0.053 resulting from independent samples t -test”.

L171. Why 24h back trajectories and not more? What is known about PBM lifetime in the Chinese boundary layer? I think there is a discussion in Horowitz et al., ACP, 2017 on this.

--Per your suggestion, we changed to 72-h back trajectories in the revised manuscript. The results of such 72-h back trajectory frequencies are shown below in Figure R1, indicating that the dominant air masses (over 90%) of source directions estimated from 72-h approach were very similar to those estimated using the 24-h and 48-h approaches.

NOAA HYSPLIT MODEL - TRAJECTORY FREQUENCIES

endpts per grid sq./# trajectories (%) 0 m and 99999 m
 Integrated from 1400 15 Oct to 1700 15 Sep 15 (UTC) [backward]
 Freq Calculation started at 0000 00 00 (UTC)



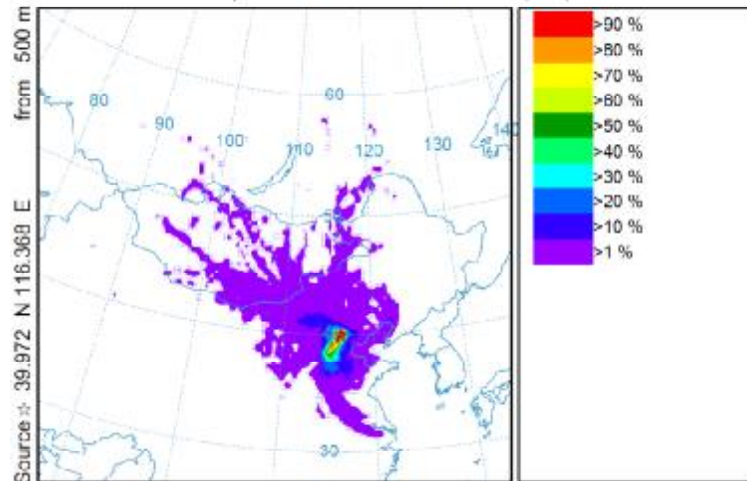
METEOROLOGICAL DATA

Job ID: 145300 Job Start: Thu Oct 15 14:07:38 UTC 2015
 Source 1 lat: 39.972500 lon: 116.368100 height: 500 m AGL
 Initial trajectory started: 1400Z 15 Oct 15
 Direction of trajectories: Backward Trajectory Duration: 24 hrs
 Frequency grid resolution: 0.50 x 0.50 degrees
 Endpoint output frequency: 60 per hour
 Number of trajectories used for this calculation: 240
 Meteorology: 0000Z 16 Oct 2015 - CDAS05b

24 hrs

NOAA HYSPLIT MODEL - TRAJECTORY FREQUENCIES

endpts per grid sq./# trajectories (%) 0 m and 99999 m
 Integrated from 1400 16 Oct to 1700 14 Sep 15 (UTC) [backward]
 Freq Calculation started at 0000 00 00 (UTC)



METEOROLOGICAL DATA

Job ID: 10444 Job Start: Sun Oct 21 13:49:51 UTC 2018
 Source 1 lat: 39.972500 lon: 116.368100 height: 500 m AGL
 Initial trajectory started: 1400Z 16 Oct 15
 Direction of trajectories: Backward Trajectory Duration: 48 hrs
 Frequency grid resolution: 0.50 x 0.50 degrees
 Endpoint output frequency: 60 per hour
 Number of trajectories used for this calculation: 280
 Meteorology: 0000Z 16 Oct 2015 - GDAS05b

48 hrs

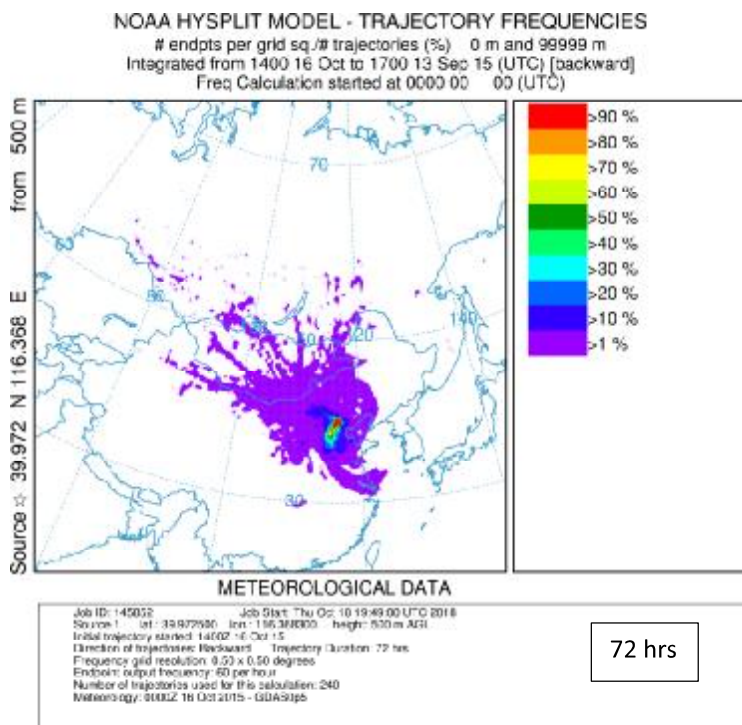


Figure R1. The frequencies of backward trajectories were calculated for all the samples using the 24h, 48h and 72h Backward Trajectory Model.

L342. “Interestingly, negative D199Hg values in daytime PM_{2.5}-Hg were only observed during a rainy day and an extreme smog event. Scavenging of locally produced GOM during rain or smog events may therefore have contributed to the reversal of the odd-MIF signature of Hg collected as PM_{2.5} at these times.” Why would local GOM have a negative D199? Not clear to reader.

--We have revised these sentences for clarity (see the revised manuscript on line 341 to 346):

“Interestingly, negative $\Delta^{199}\text{Hg}$ values in daytime PM_{2.5}-Hg were only observed during a rainy day and an extreme smog event. Since the Hg emitted from local sources had close to zero and negative values of odd-MIF, higher humidity (such as during rainy days) and heavy pollution (the extreme smog) may enhance the effect of scavenging of locally produced gaseous or

particulate Hg during rain or smog events, which may therefore have contributed to the reversal of the odd-MIF signature of Hg collected as PM_{2.5} at these times”.

2 Anonymous Referee #2

Received and published: 19 October 2018

This manuscript quantified the diel variation of Hg isotope composition of particulate bound mercury (PBM) and revealed that daily photochemical reduction of divalent Hg is of critical importance to the fate of PM_{2.5}-Hg in urban atmospheres. The topic is quite interesting and is important for understanding global mercury cycling. Publication is suggested after minor revision.

--Thank you for your comments.

Line 114 Is one air sampler enough? PBM concentration in the air is quite small. To obtain enough mercury for isotope analysis, especially when the sampling time was reduced, it seems that we need more samplers.

--We used one sampler for collecting the PM samples. Among the 61 PM_{2.5} samples we collected, 56 had sufficient Hg mass for Hg isotope analysis. It would be better if two or more samplers were used simultaneously for sampling so that (1) sufficient mass of PBM can be obtained for isotope analysis and (2) replicates could be used for isotope analysis.

Line 163 Why do you choose the height of 500 m?

--In our back trajectory modeling, we used 500 m as the average boundary layer height in Beijing according to a prior study by (Xiang et al., 2019). The estimated backward HYSPLIT trajectories of air masses should be acceptable. Alternatively, we also used different arrival heights (200, 500, 1000 m above ground level) for estimating the backward trajectories. The

results (see below Figure R2) indicate that the transport pathways are not very sensitive to the selected heights within the studied area.

Per your comments, we have added detail information in the revised version of the Supporting Information.

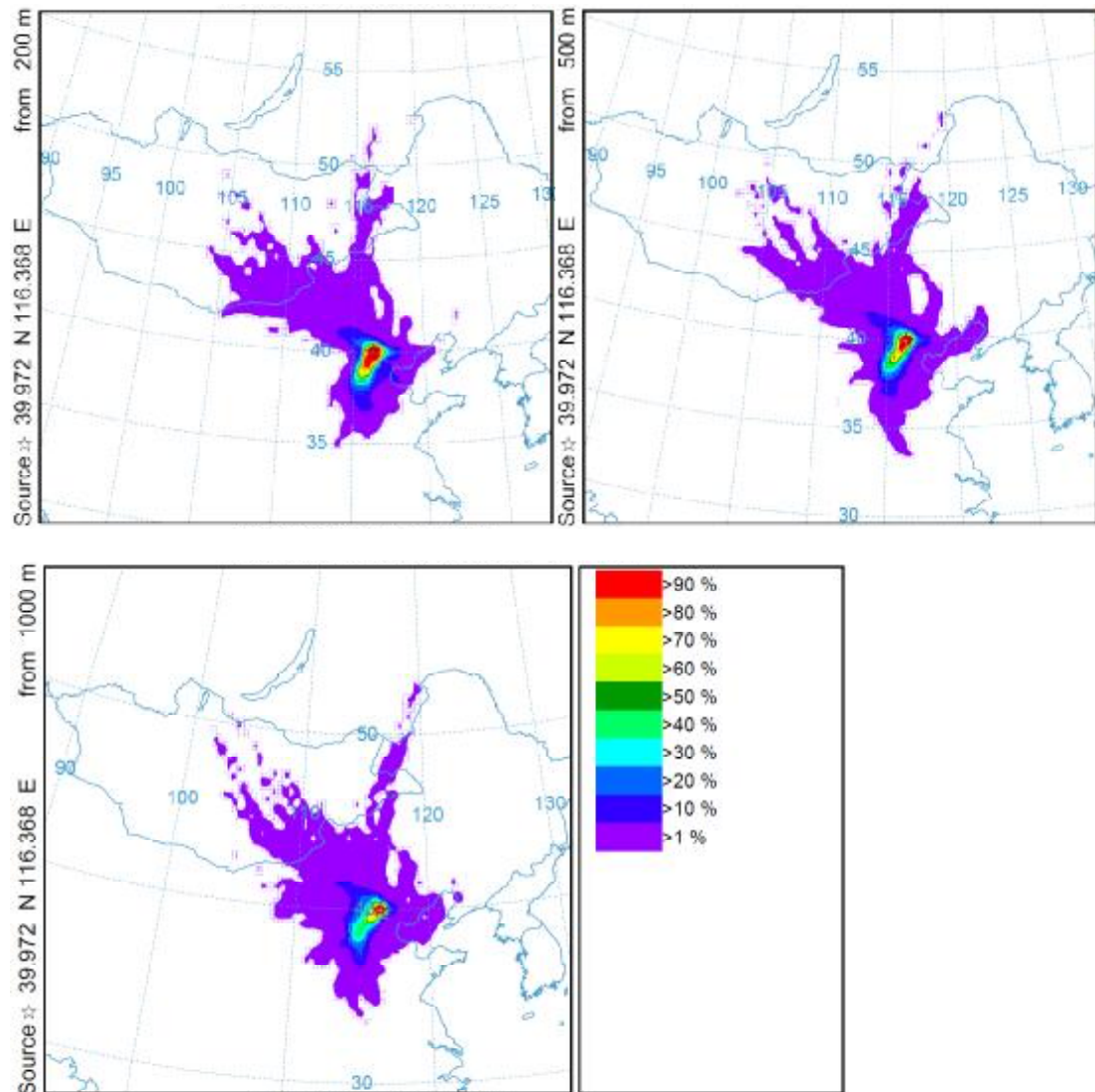


Figure R2. The frequencies of backward trajectories were calculated for all the samples using the 24h Backward Trajectory Model at three different heights of 200, 500 and 1000 m above ground level.

Figure 2 This figure is too busy. Instead listing all data according to time series, is it possible to classify the figure into several subgroup according to the topic you wants to discussed? This figure can be moved to supporting information.

--Per your suggestion, we have revised Figure 2 as following (see below Figure R3), which shows the chronological sequence of MIF ($\Delta^{199}\text{Hg}$ and $\Delta^{200}\text{Hg}$) and MDF ($\delta^{202}\text{Hg}$) of the 56 samples collected during the daytime (D, red) and nighttime (N, blue), along with selected weather data including cumulative hours of sunshine (Solar) and air mass backward-trajectory directions.

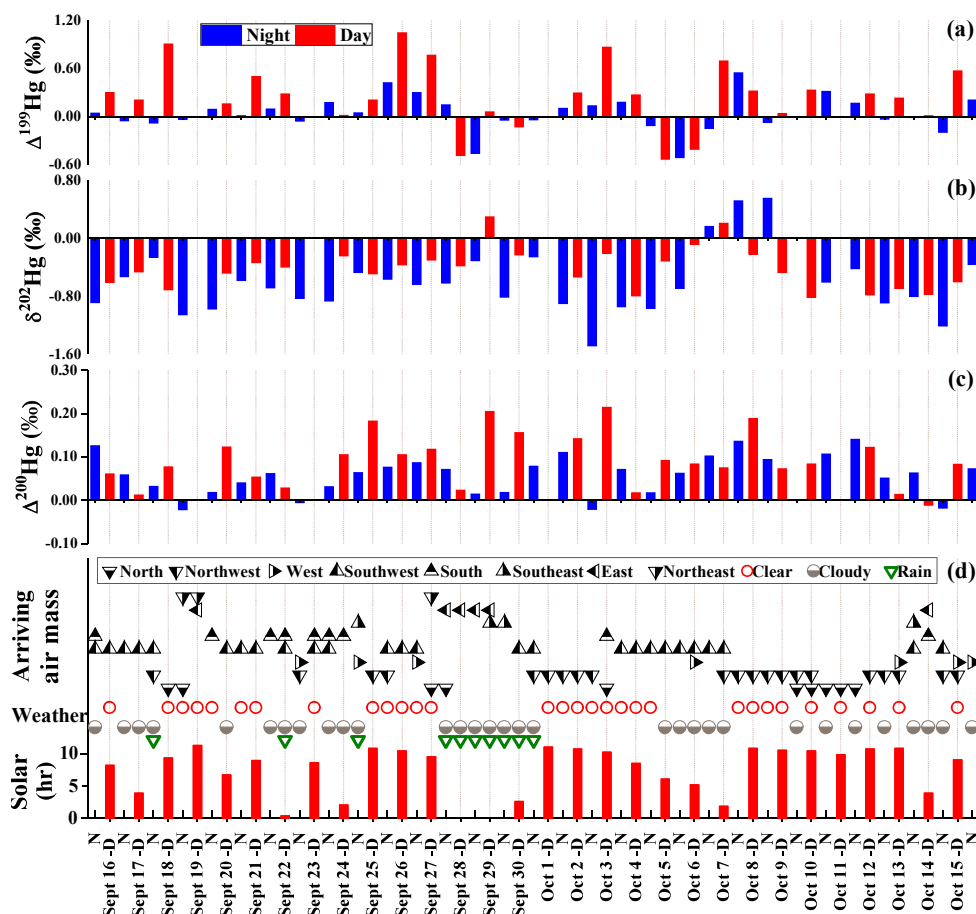


Figure R3. Chronological sequence of MIF ($\Delta^{199}\text{Hg}$ and $\Delta^{200}\text{Hg}$) and MDF ($\delta^{202}\text{Hg}$) of the 56 samples collected during the daytime (D, red) and nighttime (N, blue), along with selected

weather data including cumulative hours of sunshine (Solar) and air mass backward-trajectory directions.

Figure 2(a) How to explain the negative value of $\Delta^{199}\text{Hg}$ on Sep 28?

--The explanation had been described in Line 363 to 373. “Interestingly, negative $\Delta^{199}\text{Hg}$ values in daytime $\text{PM}_{2.5}\text{-Hg}$ were only observed during a rainy day and an extreme smog event. Since the Hg emitted from local sources had close to zero and negative values of odd-MIF, higher humidity (such as during rainy days) and heavy pollution (the extreme smog) may enhance the effect of scavenging of locally produced gaseous or particulate Hg during rain or smog events, which may therefore have contributed to the reversal of the odd-MIF signature of Hg collected as $\text{PM}_{2.5}$ at these times. In addition, the negative $\Delta^{199}\text{Hg}$ values in $\text{PM}_{2.5}$ may have resulted from the contribution of biomass burning with limited photoreduction effect during periods of less sunshine (Fig. 2 and Table S1) since plant foliage has negative $\Delta^{199}\text{Hg}$ values (Yu et al., 2016) and more negative $\Delta^{199}\text{Hg}$ values (down to -0.53%) of $\text{PM}_{2.5}\text{-Hg}$ in Beijing were related to biomass burning, a source of $\text{PM}_{2.5}\text{-Hg}$ south of Beijing in autumn (Huang et al., 2016).”

Figure 2(f) all legends are suggested to be listed on the top of this figure. It is difficult to find “clear” “cloudy” “rain” in this figure.

--We have revised the legends in the revised Figure 2(d).

Line 356 “While our results cannot exclude the effects of other possible processes, such as oxidation, adsorption (and desorption), and precipitation, based on the limited previous studies (Jiskra et al., 2012; Smith et al., 2015; Sun et al., 2016), these processes are not likely to be

important to the diel variation of odd-MIF of Hg isotopes in PM_{2.5}-Hg we observed.” The observed isotope fractionation is a phenomenon while the photochemical reduction is one process leading to this phenomenon. How can you exclude the impact from other processes? Evidences are required to prove this conclusion.

--We agree that these observations may be the result of multiple processes. We now address the possible contributions of two additional physical process, adsorption of GOM to PM and reduced boundary layer mixing of PBM at night (see responses to Referee 1).

Figure 5(a) What is the main reason that caused the variation of $\Delta^{199}\text{Hg}$ during the night time? Is it possible caused by measurement error? If this is true, it is better to point out this in method part.

--Our data showed that the $\Delta^{199}\text{Hg}$ values ranged from 0.01‰ to 0.30‰ for the nighttime samples in Figure 5(a) and ranged from -0.51‰ to 0.55‰ for all nighttime samples in this study. The method we used for quantifying Hg isotopes bears an uncertainty (2SD) of 0.06‰ for $\Delta^{199}\text{Hg}$ for the samples. Statistically, differences between $\Delta^{199}\text{Hg}$ values for daytime and nighttime samples were clearly significant and should not have been caused by uncertainty of the method. To help readers understand this issue, we have added the measurement uncertainty in the caption of Figure 5.

Reference:

Amos, H. M., Jacob, D. J., Holmes, C. D., Fisher, J. A., Wang, Q., Yantosca, R. M., Corbitt, E. S., Galarnau, E., Rutter, A. P., Gustin, M. S., Steffen, A., Schauer, J. J., Graydon, J. A., St Louis, V. L., Talbot, R. W., Edgerton, E. S., Zhang, Y., and Sunderland, E. M.: Gas-particle partitioning of atmospheric Hg(II) and its effect on global mercury deposition, *Atmos. Chem. Phys.*, 12, 591-603, 2012.

- Huang, Q., Chen, J., Huang, W., Fu, P., Guinot, B., Feng, X., Shang, L., Wang, Z., Wang, Z., Yuan, S., Cai, H., Wei, L., and Yu, B.: Isotopic composition for source identification of mercury in atmospheric fine particles, *Atmos. Chem. Phys.*, 16, 11773-11786, 2016.
- Jiskra, M., Wiederhold, J. G., Bourdon, B., and Kretzschmar, R.: Solution speciation controls mercury isotope fractionation of Hg(II) sorption to goethite, *Environ. Sci. Technol.*, 46, 6654-6662, 2012.
- Lan, X., Talbot, R., Castro, M., Perry, K., and Luke, W.: Seasonal and diurnal variations of atmospheric mercury across the US determined from AMNet monitoring data, *Atmos. Chem. Phys.*, 12, 10569-10582, 2012.
- Liu, B., Keeler, G. J., Dvonch, J. T., Barres, J. A., Lynam, M. M., Marsik, F. J., and Morgan, J. T.: Temporal variability of mercury speciation in urban air, *Atmos. Environ.*, 41, 1911-1923, 2007.
- Poissant, L., Pilote, M., Beauvais, C., Constant, P., and Zhang, H. H.: A year of continuous measurements of three atmospheric mercury species (GEM, RGM and Hg-p) in southern Quebec, Canada, *Atmos. Environ.*, 39, 1275-1287, 2005.
- Quan, J. N., Gao, Y., Zhang, Q., Tie, X. X., Cao, J. J., Han, S. Q., Meng, J. W., Chen, P. F., and Zhao, D. L.: Evolution of planetary boundary layer under different weather conditions, and its impact on aerosol concentrations, *Particuology*, 11, 34-40, 2013.
- Rutter, A. P., and Schauer, J. J.: The effect of temperature on the gas-particle partitioning of reactive mercury in atmospheric aerosols, *Atmos. Environ.*, 41, 8647-8657, 2007.
- Smith, R. S., Wiederhold, J. G., and Kretzschmar, R.: Mercury isotope fractionation during precipitation of metacinnabar (β -HgS) and montroydite (HgO), *Environ. Sci. Technol.*, 49, 4325-4334, 2015.
- Xiang, Y., Zhang, T., Liu, J., Lv, L., Dong, Y., and Chen, Z.: Atmosphere boundary layer height and its effect on air pollutants in Beijing during winter heavy pollution, *Atmos. Res.*, 215, 305-316, <https://doi.org/10.1016/j.atmosres.2018.09.014>, 2019.
- Yu, B., Fu, X., Yin, R., Zhang, H., Wang, X., Lin, C.-J., Wu, C., Zhang, Y., He, N., Fu, P., Wang, Z., Shang, L., Sommar, J., Sonke, J. E., Maurice, L., Guinot, B., and Feng, X.: Isotopic composition of atmospheric mercury in China: New evidence for sources and transformation processes in air and in vegetation, *Environ. Sci. Technol.*, 50, 9262-9269, 2016.

Diel variation of mercury stable isotope ratios record photoreduction of PM_{2.5}-bound mercury

Qiang Huang^{1,2}, Jiubin Chen^{1,3,*}, Weilin Huang⁴, John R. Reinfeld⁴, Pingqing Fu⁵, Shengliu

5 Yuan¹, Zhongwei Wang¹, Wei Yuan¹, Hongming Cai¹, Hong Ren⁵, Yele Sun⁵ and Li He⁶

¹ SKLEG, Institute of Geochemistry, CAS, Guiyang 550081, China

² SKLOG, Guangzhou Institute of Geochemistry, CAS, Guangzhou 510640, China

³ Institute of Surface-Earth System Science, Tianjin University, 300072, China

⁴ Department of Environmental Sciences, Rutgers, The State University of New Jersey, New
10 Brunswick, NJ 08901, USA

⁵ LAPC, Institute of Atmospheric Physics, CAS, Beijing 100029, China

⁶ Laboratory of Hebei Institute of Regional Geology and Mineral Resources Survey,
Shijiazhuang 065000, China

*Corresponding author.

15 E-mail: jbchen@tju.edu.cn

Abstract. Mercury (Hg) bound to fine aerosols (PM_{2.5}-Hg) may undergo photochemical reaction that causes isotopic fractionation and obscures the initial isotopic signatures. In this study, we quantified Hg isotopic compositions for 56 PM_{2.5} samples collected between Sept. 15th and Oct. 16th, 2015 from Beijing, China, among which 26 were collected during the daytime (between 8:00 a.m. and 6:30 p.m.) and 30 during night (between 7:00 p.m. and 7:30 a.m.). The results show that diel variation was statistically significant ($p < 0.05$) for Hg content, $\Delta^{199}\text{Hg}$ and $\Delta^{200}\text{Hg}$, with Hg content during the daytime ($0.32 \pm 0.14 \mu\text{g g}^{-1}$) lower than at night ($0.48 \pm 0.24 \mu\text{g g}^{-1}$) and $\Delta^{199}\text{Hg}$ and $\Delta^{200}\text{Hg}$ values during the daytime (mean of $0.26\text{‰} \pm 0.40\text{‰}$ and $0.09\text{‰} \pm 0.06\text{‰}$, respectively) higher than during the nighttime ($0.04\text{‰} \pm 0.22\text{‰}$ and $0.06\text{‰} \pm 0.05\text{‰}$, respectively), whereas PM_{2.5} concentrations and $\delta^{202}\text{Hg}$ values showed insignificant ($p > 0.05$) diel variation. Geochemical characteristics of the samples and the air mass backward trajectories (PM_{2.5} source related) suggest that diel variation in $\Delta^{199}\text{Hg}$ values resulted primarily from the photochemical reduction of divalent PM_{2.5}-Hg, rather than variations in emission sources. The importance of photoreduction is supported by the strong correlations between $\Delta^{199}\text{Hg}$ and: (i) $\Delta^{201}\text{Hg}$ (positive, slope = 1.1), (ii) $\delta^{202}\text{Hg}$ (positive, slope = 1.15), (iii) content of Hg in PM_{2.5} (negative), (iv) sunshine durations (positive), and (v) ozone concentration (positive) observed for consecutive day-night paired samples. Our results provide isotopic evidence that local, daily photochemical reduction of divalent Hg is of critical importance to the fate of PM_{2.5}-Hg in urban atmospheres and that, in addition to variation in sources, photochemical reduction appears to be an important process that affects both the particle mass-specific abundance and isotopic composition of PM_{2.5}-Hg.

Keywords: Mass-independent fractionation; Atmospheric particulate mercury; Transport and transformation; Isotopic evidence of photoreduction

1 Introduction

40 Atmospheric mercury (Hg) consists of three operationally-defined forms including particle-bound Hg (PBM), gaseous oxidized Hg (GOM), and gaseous elemental Hg (GEM) (Selin, 2009). GEM is the most abundant (about 90%) and chemically stable form (Selin, 2009), and is transported at regional and global scales. GOM has short residence times as it can readily be dissolved in rain droplets, adsorbed on particulate matter (PM), and it reacts rapidly within both
45 gaseous and aqueous phases with or without PM. PBM contains mainly reactive Hg species such as Hg^{2+} and perhaps trace quantities of Hg^0 , and is transported at regional or local scales thereby reflecting Hg pollution and cycling within short distances from emission source (Selin, 2009; Subir et al., 2012). PBM has multiple sources and undergoes complex transport and transformation processes in the atmosphere (Subir et al., 2012).

50 This study aimed at characterizing the isotope compositions of $\text{PM}_{2.5}\text{-Hg}$ (particulate matter with aerodynamic diameter less than 2.5 micrometers) to better understand the complex transformation processes of PBM. Hg has seven stable isotopes and is known to exhibit both mass-dependent (MDF, represented by $\delta^{202}\text{Hg}$) and mass-independent (MIF, including odd-mass-number isotopic MIF (odd-MIF) and even-mass-number isotopic MIF (even-MIF),
55 represented by $\Delta^{199}\text{Hg}$, $\Delta^{201}\text{Hg}$, $\Delta^{200}\text{Hg}$ and $\Delta^{204}\text{Hg}$) fractionation during Hg transformations under various environmental conditions (Hintelmann and Lu, 2003; Jackson et al., 2004; Bergquist and Blum, 2007; Jackson et al., 2008; Gratz et al., 2010; Chen et al., 2012; Sherman et al., 2012). Prior studies have shown that MDF can be induced by several Hg transformation and transport processes (Bergquist and Blum, 2007; Kritee et al., 2007; Estrade et al., 2009;
60 Yang and Sturgeon, 2009; Sherman et al., 2010; Wiederhold et al., 2010; Ghosh et al., 2013; Smith et al., 2015; Janssen et al., 2016), but large extents of odd-MIF mainly occurred during photochemical reactions including photoreduction (Bergquist and Blum, 2007; Zheng and Hintelmann, 2009; Sherman et al., 2010; Zheng and Hintelmann, 2010b; Rose et al., 2015),

photodemethylation (Bergquist and Blum, 2007; Rose et al., 2015) and photooxidation (Sun et al., 2016). Smaller but measurable degrees of odd-MIF were also reported for nonphotochemical abiotic reduction (Zheng and Hintelmann, 2010a) and evaporation of Hg^0 (Estrade et al., 2009; Ghosh et al., 2013). Interestingly, the results of laboratory and field investigations suggest that specific $\Delta^{199}\text{Hg}/\Delta^{201}\text{Hg}$ ratios are associated with such transformation processes, with a ratio of about 1.0 for photoreduction of inorganic Hg^{2+} (Bergquist and Blum, 2007; Zheng and Hintelmann, 2009; Sherman et al., 2010; Zheng and Hintelmann, 2010b; Rose et al., 2015), about 1.3 for photodemethylation and 1.6 for Hg^0 evaporation and photooxidation (Bergquist and Blum, 2007; Estrade et al., 2009; Zheng and Hintelmann, 2010a; Ghosh et al., 2013; Rose et al., 2015; Sun et al., 2016). Even-MIF of Hg isotope signatures were observed mostly in wet deposition, but the mechanism producing such fractionation remains unknown (Chen et al., 2012; Cai and Chen, 2016).

Prior studies have shown relatively constant Hg isotope compositions for GEM and very large variations of Hg isotope ratios for dissolved Hg^{2+} in wet precipitation (Gratz et al., 2010; Chen et al., 2012; Rolison et al., 2013; Wang et al., 2015; Yuan et al., 2015). A few studies reported that the Hg isotope compositions of PBM also show large variations (Rolison et al., 2013; Das et al., 2016; Huang et al., 2016; Yu et al., 2016; Xu et al., 2017). Among these limited studies, Rolison et al. (2013) reported $\delta^{202}\text{Hg}$ (-1.61‰ to -0.12‰) and $\Delta^{199}\text{Hg}$ values (0.36‰ to 1.36‰) for Hg bound on total suspended particulates (TSP), with $\Delta^{199}\text{Hg}/\Delta^{201}\text{Hg}$ ratios of approximately unity, a value typical of photoreduction of inorganic Hg^{2+} . Das et al. (2016) found values of $\Delta^{199}\text{Hg}$ varied between -0.31‰ and 0.33‰ for PM_{10} from Kolkata, eastern India. It was suggested that PBM with longer residence times may have undergone greater photoreduction and hence exhibited more positive MIF. Huang et al. (2016) investigated Hg isotope compositions for $\text{PM}_{2.5}$ samples taken from Beijing, China, and attributed their observed seasonal variations in both MDF ($\delta^{202}\text{Hg}$ from -2.18‰ to 0.51‰) and MIF ($\Delta^{199}\text{Hg}$

from -0.53‰ to 0.57‰) to varied contributions from multiple sources of $\text{PM}_{2.5}\text{-Hg}$, while the
90 more positive $\Delta^{199}\text{Hg}$ values were likely produced by extensive photochemical reduction during
long-range-transported. These prior results show that the Hg isotope approach can be employed
for tracking sources and identifying possible transformation processes for airborne PM-Hg, and
that PBM may undergo photochemical reactions that obscure its initial isotopic signature.

The goal of this study was to quantify short-term (diel) variations in the isotope composition
95 of $\text{PM}_{2.5}\text{-Hg}$ in an effort to elucidate if photochemical processes could impact overall contents
and isotope compositions of PM-bound Hg in an urban environment. Unlike prior studies in
which PM samples were collected continuously over 24 hrs or longer, we collected two $\text{PM}_{2.5}$
samples per 24 hrs with a daytime (D) sample between 8:00 a.m. and 6:30 p.m. and a nighttime
(N) sample between 7:00 p.m. and 7:30 a.m.- ~~It is intuitive that, while both D and N $\text{PM}_{2.5}$
100 samples may have similar local or regional sources if the wind trajectory remains unchanged,
D samples could have been exposed to more solar radiation than N samples, likely resulting in
diel variations in the Hg isotope compositions that are indicative of differences in
photochemical transformation of $\text{PM}_{2.5}\text{-Hg}$.~~ The specific objectives of this study were to verify
and quantify whether Hg isotope compositions of $\text{PM}_{2.5}$ exhibit diel variations, and to elucidate
105 whether photochemical transformation is the dominant process for such diel variations.

2 Experimental section

2.1 Field site, sampling method, and preconcentration of $\text{PM}_{2.5}\text{-Hg}$

Beijing was selected as the area of study because of its well-known air pollution issue (Zhang
110 et al., 2007). Detailed information on the study site and $\text{PM}_{2.5}$ sampling procedures were given
elsewhere (Huang et al., 2016). During the sampling period between Sept. 15th and Oct. 16th,
2015, the average outdoor temperatures were $22.1 \pm 3.0^\circ\text{C}$ and $18.5 \pm 2.7^\circ\text{C}$, and the average
relative humidity were $45 \pm 20\%$ and $59 \pm 19\%$, for D and N, respectively. The $\text{PM}_{2.5}$ samples

were collected using a Tisch Environmental PM_{2.5} high volume air sampler, which collects
115 particles at a flow rate of 1.0 m³ min⁻¹ through a PM_{2.5} size selective inlet on a pre-combusted
(450°C for 6 hrs) quartz fiber filter (Pallflex 2500 QAT-UP, 20 cm × 25 cm, Pallflex Product
Co., USA). Quartz fiber filters were widely used to collect operationally defined PBM
(Schleicher et al., 2015; Zhang et al., 2015; Xu et al., 2017). A total of 61 samples including 30
D samples and 31 N samples were collected between 8:00 a.m. and 6:30 p.m. and 7:00 p.m. to
120 7:30 a.m., respectively, along with 2 field blanks. They were wrapped with aluminum film,
packed in plastic bags, and stored at -20°C in the lab prior to analysis. Meteorological data,
including temperature (T), relative humidity (RH), sunshine duration, daily average wind speed
(WS), were acquired from China Meteorological Administration (<http://data.cma.cn>), and the
atmospheric ozone content (*P*_{O₃}) was measured concurrently. These data are summarized in
125 Table S1.

2.2 Hg content and stable isotope measurements

The mass of each PM_{2.5} sample was gravimetrically quantified. Hg bound on each PM_{2.5} sample
was extracted and concentrated for analysis of Hg content and stable Hg isotopes using the
method reported previously (Huang et al., 2015). The details of the procedures are also given
130 in supplementary material (SI).

Among the 61 PM_{2.5} samples, 56 (including 26 D- and 30 N-samples) had sufficient Hg mass
(> 10 ng) and were further analyzed for Hg isotope compositions using a multicollector
inductively coupled plasma mass spectrometer (MC-ICP-MS, Nu Instruments Ltd., UK)
equipped with a continuous flow cold vapor generation system. Detailed protocols for the Hg
135 isotope analysis can be found in Huang et al. (2015) and also in SI. ¹⁹⁶Hg and ²⁰⁴Hg were not
measured due to their very low abundance. Instrumental mass bias was corrected using an
internal standard (NIST SRM 997 Tl) and strict sample-standard bracketing with NIST SRM

3133 Hg standard. Delta (δ) notation is used to represent MDF in units of per mil (‰) as defined by the following equation (Blum and Bergquist, 2007):

$$\delta^x\text{Hg} (\text{‰}) = [({}^x\text{Hg}/{}^{198}\text{Hg})_{\text{sample}}/({}^x\text{Hg}/{}^{198}\text{Hg})_{\text{NIST3133}} - 1] \times 1000 \quad (1)$$

where $x = 199, 200, 201,$ and 202 . MIF is reported as the deviation of a measured delta value from the theoretically predicted MDF value according to the equation:

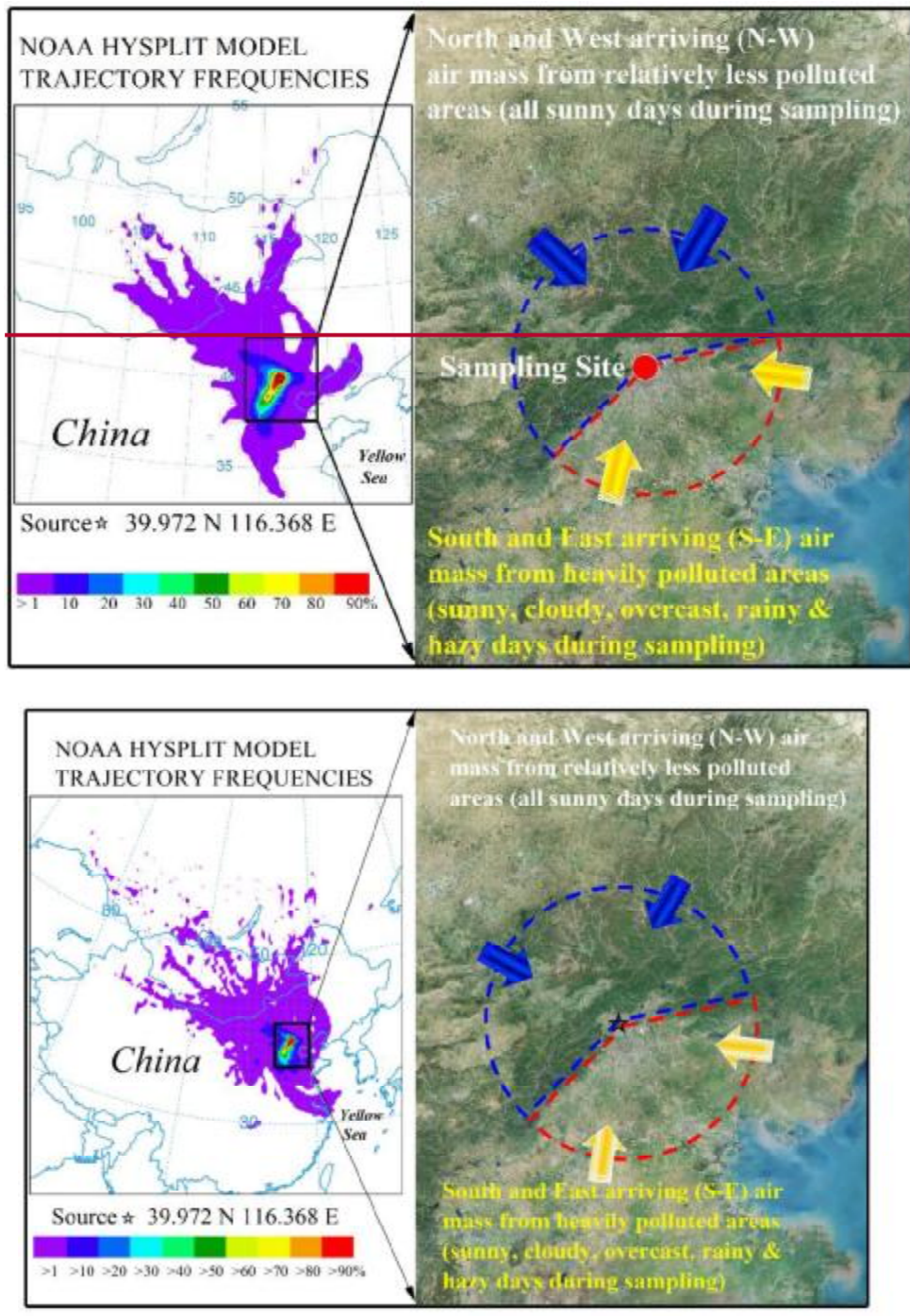
$$\Delta^x\text{Hg} (\text{‰}) = \delta^x\text{Hg} - \beta \times \delta^{202}\text{Hg} \quad (2)$$

where the mass-dependent scaling factor β is 0.252, 0.5024, and 0.752 for ${}^{199}\text{Hg}$, ${}^{200}\text{Hg}$ and ${}^{201}\text{Hg}$, respectively (Blum and Bergquist, 2007).

For quality assurance and control, we used NIST SRM 3177 Hg as a secondary standard and analyzed repeatedly during sample analysis session. The collective measurements of the NIST 3177 standard yielded average $\delta^{202}\text{Hg}$, $\Delta^{199}\text{Hg}$, $\Delta^{200}\text{Hg}$ and $\Delta^{201}\text{Hg}$ values of $-0.53\text{‰} \pm 0.09\text{‰}$, $-0.01\text{‰} \pm 0.04\text{‰}$, $0.00\text{‰} \pm 0.04\text{‰}$ and $-0.01\text{‰} \pm 0.07\text{‰}$ (2SD, $n = 17$). We also analyzed regularly a well-known reference material UM-Almaden and a certified reference material (CRM) GBW07405, and the results showed average $\delta^{202}\text{Hg}$, $\Delta^{199}\text{Hg}$, $\Delta^{200}\text{Hg}$ and $\Delta^{201}\text{Hg}$ values of $-0.60\text{‰} \pm 0.09\text{‰}$, $-0.01\text{‰} \pm 0.04\text{‰}$, $0.01\text{‰} \pm 0.04\text{‰}$ and $-0.03\text{‰} \pm 0.07\text{‰}$ (2SD, $n = 17$) and of $-1.77\text{‰} \pm 0.14\text{‰}$, $-0.29\text{‰} \pm 0.06\text{‰}$, $0.00\text{‰} \pm 0.04\text{‰}$ and $-0.32\text{‰} \pm 0.07\text{‰}$ (2SD, $n = 6$), respectively. These values were consistent with previous results (Blum and Bergquist, 2007; Chen et al., 2010; Huang et al., 2015; Huang et al., 2016). The uncertainties of $\text{PM}_{2.5}\text{-Hg}$ isotope ratios listed in Table S2 were calculated based on repetitive measurements. However, if uncertainty of the isotopic compositions for a given sample was smaller than the uncertainty of CRM GBW07405, the uncertainty associated with that sample was assigned 2SD uncertainties (0.14‰, 0.06‰, 0.04‰ and 0.07‰ for $\delta^{202}\text{Hg}$, $\Delta^{199}\text{Hg}$, $\Delta^{200}\text{Hg}$ and $\Delta^{201}\text{Hg}$) obtained for long-term measurement of the CRM GBW07405.

2.3 Air mass backward trajectories

To identify possible pathways of PM_{2.5}-Hg transport, backward HYSPLIT trajectories of air masses at a height of 500 m above ground level and arriving at the sampling site were simulated. Backward trajectories for each D or N sample were calculated every 1 hrs using the Internet-
165 Based HYSPLIT Trajectory Model and gridded meteorological data (Global Data Assimilation System, GDAS1) from the U.S. National Oceanic and Atmospheric Administration (NOAA) (Fig. S1). The obtained average directions of arriving air masses for each sample were summarized in Table S1. The frequencies of backward trajectories were calculated for all the samples taken during Sept. 15th to Oct. 16th 2015 using the Internet-Based HYSPLIT Trajectory
170 Model and the archived GDAS0p5, with an interval of 3 hrs. Each trajectory had a total run time of 24-72 hrs and a grid resolution of 0.5 × 0.5 degree trajectory frequency. The simulation results showed the dominant air mass was arriving from southwest of the sampling site during the sampling period (see Fig. 1).



175

Figure 1. Geographic location of the PM_{2.5} collection site in Beijing, China (Baidu Map image) and average air mass back trajectories during sampling from Sept. 15th to Oct. 16th, 2015 (left), and characteristics of North-West vs. South-East arriving air masses.

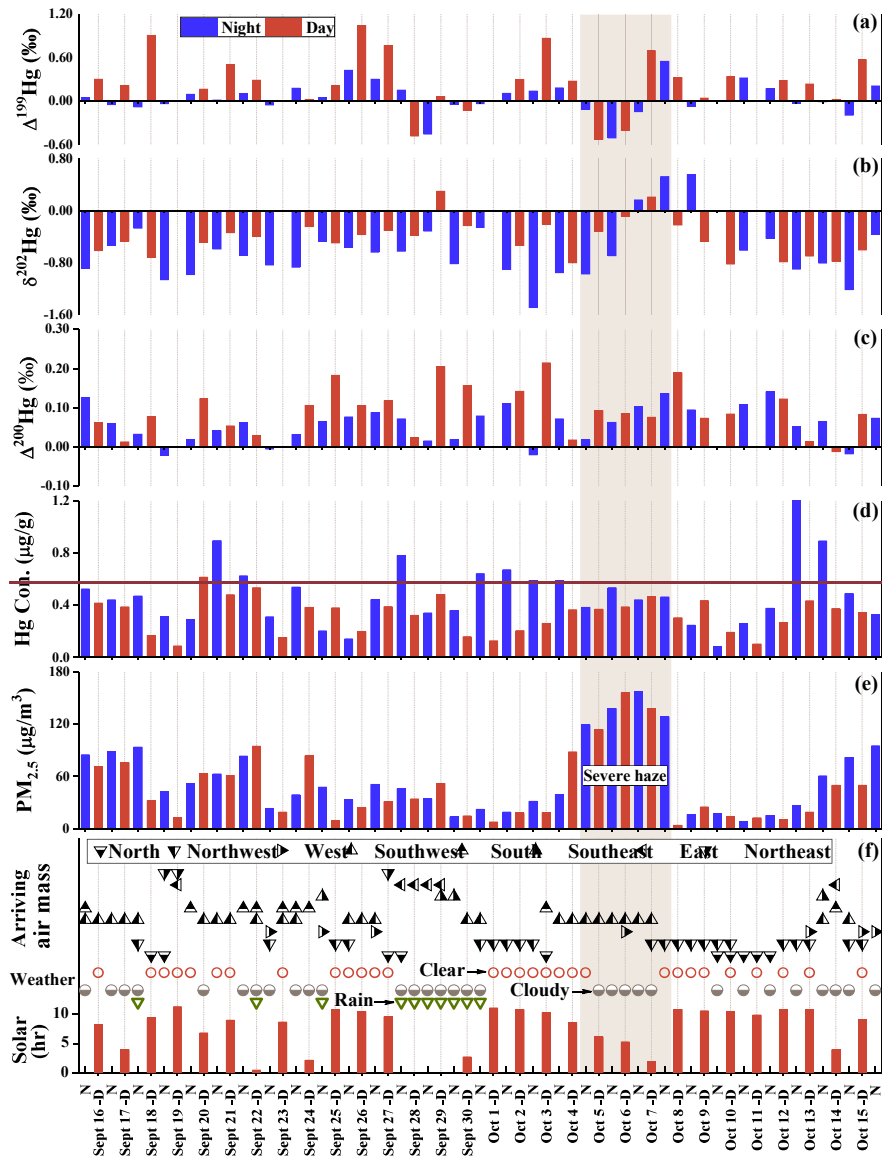
2.4 Statistical analysis

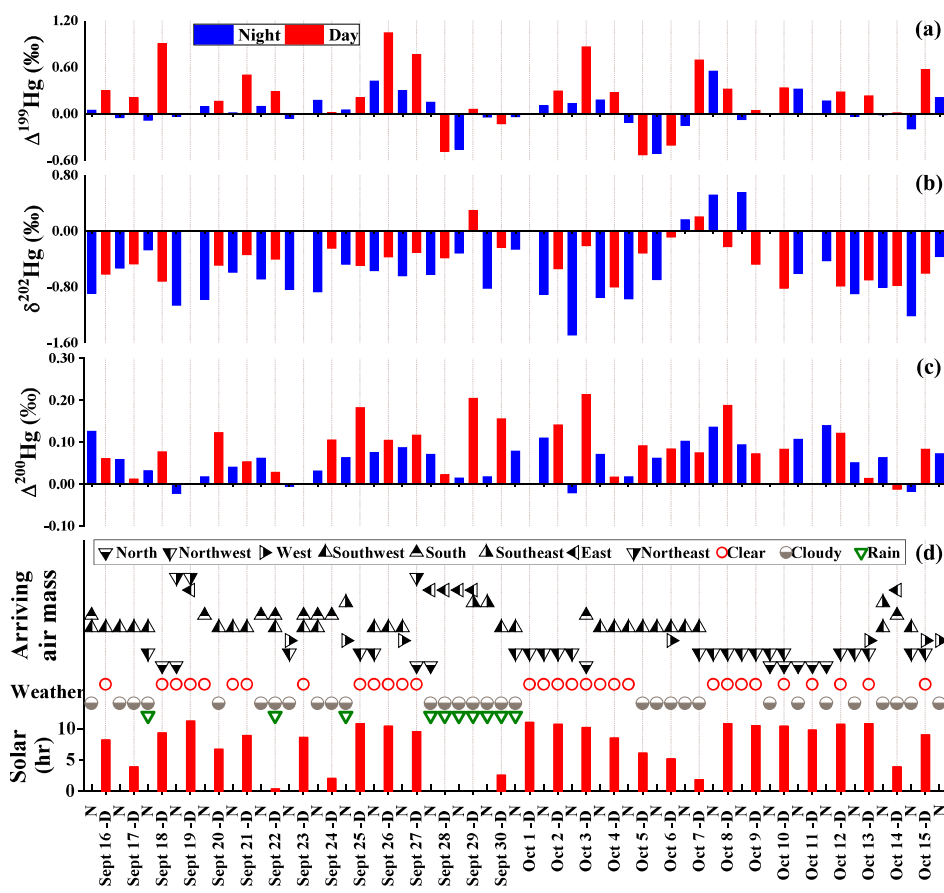
180 T-test was performed for uncertainty analysis using IBM SPSS Statistics Version 22. Both
| ~~Paired-paired Samples-samples T_t -test~~ and ~~Independent-independent Samples-samples T_t -test~~
were performed for diel variations of Hg content, $\delta^{202}\text{Hg}$, $\Delta^{199}\text{Hg}$ and $\Delta^{200}\text{Hg}$, and their results
were summarized in Table S3.

185 **3 Results and discussion**

3.1 Diel variation of PM_{2.5}-Hg

| The chronological sequence of Hg stable isotope ratios, along with ~~PM_{2.5} sample properties and~~
weather conditions for the 56 PM_{2.5} samples are presented in Figure 2 (see also Tables S1 and
S2 for quantitative atmospheric data and $\Delta^{201}\text{Hg}$ values). The major features of this dataset
190 include: i) large variations in both MDF and odd-MIF of Hg isotopes, ii) significant diel
differences in Hg isotope ratios, iii) correlations of weather conditions and air mass backward
trajectories with Hg isotope signals, and iv) detectable even-MIF.





195 **Figure 2.** Chronological sequence of MIF ($\Delta^{199}\text{Hg}$ and $\Delta^{200}\text{Hg}$) and, MDF ($\delta^{202}\text{Hg}$), PM_{2.5}-Hg contents (C_{Hg}), and PM_{2.5}-concentrations of the 56 samples collected during the daytime (D, red) and nighttime (N, blue), along with selected weather data including cumulative hours of sunshine (Solar) and air mass backward-trajectory directions.

200 The volumetric PM_{2.5} concentrations ranged from 4 to 158 $\mu\text{g m}^{-3}$ with an average value of $52 \pm 40 \mu\text{g m}^{-3}$ (1SD, $n = 61$) and the highest values ($> 100 \mu\text{g m}^{-3}$) detected during a severe haze event of Oct. 4th-7th. The mass-based Hg contents ranged from 0.08 to 1.22 $\mu\text{g g}^{-1}$ with a mean value of $0.40 \pm 0.21 \mu\text{g g}^{-1}$ (1SD, $n = 61$).

Hg isotope analysis showed that $\delta^{202}\text{Hg}$ values varied from -1.49‰ to 0.55‰ (mean = -0.53‰ $\pm 0.40\text{‰}$, 1SD, $n = 56$), with the lowest value found in sample Oct-2-N and the highest in Oct-8-N. Significant odd-MIF of Hg isotopes was found and the $\Delta^{199}\text{Hg}$ values ranged from -0.53‰ to 1.04‰ (mean = $0.14\text{‰} \pm 0.33\text{‰}$) with the lowest (-0.53‰) $\Delta^{199}\text{Hg}$ value on Oct-5-D during

the severe haze event and the highest (1.04‰) $\Delta^{199}\text{Hg}$ value on Sept-26-D during a sunny day (without cloud) (Fig. 2). All samples also displayed slight even-MIF, with $\Delta^{200}\text{Hg}$ values ranging from -0.02‰ to 0.21‰ (average $0.07\text{‰} \pm 0.06\text{‰}$, 1SD, $n = 56$), which were significant compared to the detection precision of $\pm 0.04\text{‰}$. The overall variations of Hg isotope ratios for these 12-hr D/N $\text{PM}_{2.5}$ samples are generally consistent with several prior reports for the 24-hr PBM samples (Rolison et al., 2013; Das et al., 2016; Huang et al., 2016).

T-test results (Table S3) showed that diel variation was statistically significant ($p < 0.05$) for Hg contents, $\Delta^{199}\text{Hg}$, and $\Delta^{200}\text{Hg}$ values, as their p values are 0.005, 0.000 and 0.004 resulting from paired samples t -test, and are 0.003, 0.017 and 0.019 resulting from independent samples t -test. For all samples, Hg contents for D-samples ($0.32 \pm 0.14 \mu\text{g g}^{-1}$) were lower than N-samples ($0.48 \pm 0.24 \mu\text{g g}^{-1}$), and $\Delta^{199}\text{Hg}$ and $\Delta^{200}\text{Hg}$ values for D-samples (mean of $0.26\text{‰} \pm 0.40\text{‰}$ and $0.09\text{‰} \pm 0.06\text{‰}$, respectively) were higher than N-samples ($-0.04\text{‰} \pm 0.22\text{‰}$ and $0.06\text{‰} \pm 0.05\text{‰}$, respectively). However, $\text{PM}_{2.5}$ concentrations and $\delta^{202}\text{Hg}$ had statistically insignificant ($p > 0.05$) diel variation, as their p values are 0.887 and 0.052 resulting from paired samples t -test, and are 0.909 and 0.053 resulting from independent samples t -test.

3.2 Diel variation in odd-MIF of $\text{PM}_{2.5}\text{-Hg}$ independent of air mass source

Many consecutive D-N sampling intervals had similar air mass back trajectories (Table S1 and Fig. S1), suggesting that the dominant sources of $\text{PM}_{2.5}\text{-Hg}$ did not vary over each such 24 hr sampling period. For example, pairs Sept-16-D and Sept-16-N, Sept-17-D and Sept-17-N, Sept-20-D and Sept-20-N, Sept-21-D and Sept-21-N, Oct-1-D and Oct-1-N, Oct-2-D and Oct-2-N, Oct-4-D and Oct-4-N have similar air mass trajectories from the southwest, and pairs Oct-8-D and Oct-8-N, Oct-9-D and Oct-9-N, Oct-10-D and Oct-10-N, Oct-11-D and Oct-11-N, Oct-12-D and Oct-12-N have similar air mass trajectories from the northwest and north (Fig. S1). It is reasonable to assume, therefore, that each of these D-N $\text{PM}_{2.5}$ sample pairs had identical

dominant sources of PM_{2.5}-Hg and to expect that they would have very similar Hg isotope compositions. Instead, however, the data presented in Table S2 and Figure 2 revealed a unique and consistent pattern of diel variation in Hg isotope ratios; specifically, each PM_{2.5} D-sample had a statistically significantly higher positive $\Delta^{199}\text{Hg}$ value (up to +1.04‰) than its consecutive PM_{2.5} N-sample.

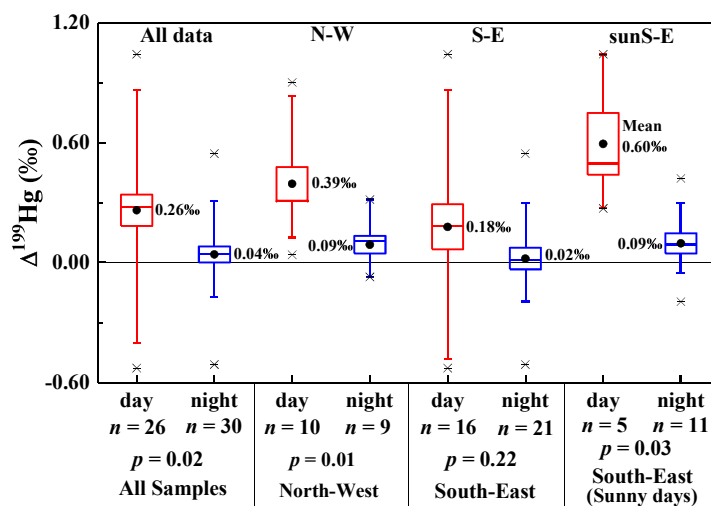
The more positive $\Delta^{199}\text{Hg}$ values measured for the PM_{2.5} D-samples are highly unlikely uncharacteristic of known emission sources of PM_{2.5}-Hg. It is possible that PM_{2.5}-Hg from different emission sources may have different Hg isotope compositions. However, prior studies showed that $\Delta^{199}\text{Hg}$ values of the PBM from dominant anthropogenic emission sources are generally negative or close to zero. Schleicher et al. (2015) demonstrated that coal combustion is likely the major source of PM_{2.5}-Hg in Beijing. Huang et al (2016) reported that regional anthropogenic activities such as coal combustion ($\Delta^{199}\text{Hg}$ values from -0.30‰ to 0.05‰), metal smelting (-0.20‰ to -0.05‰) and cement production (-0.25‰ to 0.05‰), as well as biomass burning (low to -0.53‰) were likely the dominant sources of PM_{2.5}-Hg at this study site. As shown in Figure 2 and Table S1, the PM_{2.5} D-samples with high $\Delta^{199}\text{Hg}$ values (> 0.60‰) each had very different air mass back trajectories (Fig. S1). For instance, Sept-18-D (with $\Delta^{199}\text{Hg}$ value +0.90‰), Sept-26-D (with $\Delta^{199}\text{Hg}$ value +1.04‰) and Oct-3-D (with $\Delta^{199}\text{Hg}$ value +0.86‰) were associated with north, southwest, and north-south mixed air masses, respectively. A reasonable explanation of these observations is that high positive $\Delta^{199}\text{Hg}$ values measured for D-samples resulted from PM_{2.5}-Hg transformation, specifically photoreduction, during atmospheric transport. Indeed, the diel variation of $\Delta^{199}\text{Hg}$ for PM_{2.5} D-N sample pairs may well reflect strong (D) versus less or no (N) influences of photochemical reactions under time-variant local and regional weather conditions.

3.3 Photochemical reduction as a cause of odd-MIF in subset of daytime PM_{2.5} samples

To detail the effects of photochemical reactions on the variation of Hg isotope ratios for PM_{2.5}-Hg, we regrouped our dataset into subsets corresponding to day and night. We further regrouped our results into two source-related subsets, south-east (S-E) and north-west (N-W), according to the air mass backward trajectories during each sampling event (Fig. 1), and two other subsets corresponding to sunny days within the S-E group (sunS-E) and all sunny days (Sun), which includes sunS-E and N-W as N-W consisted entirely of sunny days. The N-W subset of PM_{2.5} was associated with an air mass that tracked from the north, northeast, northwest and west, relatively less polluted areas, and is therefore representative of long-range transport and relatively constant sources of PM_{2.5} and Hg (Huang et al., 2016). The S-E subset was associated with an air mass that tracked from the south, southwest, southeast and east, heavily polluted and highly populated areas, and was characterized by relatively high contents of PM_{2.5}, likely from industrial sources in the region (coal fired power plants, coking and steel industries). Unlike the N-W arriving air mass which corresponded to all sunny days during the entire sampling period, the S-E arriving air mass was associated with a range of weather conditions including hazy, cloudy, rainy, and sunny days. According to our results (Table S2 and Fig. 2), PM_{2.5} concentrations of the N-W subset ($23 \pm 19 \mu\text{g m}^{-3}$) were significantly ($p < 0.05$) lower than the S-E subset ($69 \pm 40 \mu\text{g m}^{-3}$), which is consistent with the fact that the N-W areas of Beijing were less industrialized, less populated and less polluted than the S-E areas. However, regardless of whether their associated air masses originated from moderately or heavily polluted areas, both N-W and S-E subset samples showed diel variations in their Hg contents and isotope ratios (see Fig. 3 and discussion below). This, as discussed above, indicates that air mass source was not a dominant factor producing the diel variation of Hg isotope ratios in consecutive D-N PM_{2.5} samples.

The observed diel difference in $\Delta^{199}\text{Hg}$ values of PM_{2.5}-Hg is even more prominent and statistically robust within subsets of PM_{2.5} samples regrouped according to their air mass

trajectories (i.e., PM_{2.5} source related) and sunny days (with greater extent of photochemical reactions). As shown in Figure 3, $\Delta^{199}\text{Hg}$ values for N-W subset samples collected during the day had a higher range (0.04‰ to 0.90‰) and mean (0.39‰ \pm 0.27‰ SD, $n = 10$) compared to those (-0.07‰ to 0.32‰, mean = 0.09‰ \pm 0.13‰ SD, $n = 9$) for N-samples ($p = 0.02$). Similarly, analysis of the sunS-E subset revealed a significant difference in $\Delta^{199}\text{Hg}$ values ($p = 0.03$) between sunny days and nights, but not when the entire S-E sample set ($p = 0.22$), which includes hazy, raining, and cloudy days, was considered. Since the N-W subset was associated with less polluted areas and the S-E subset was associated with heavily polluted and highly populated areas, the observation of significant diel variation of $\Delta^{199}\text{Hg}$ in PM_{2.5}-Hg within each subset (Fig. 3) is consistent with the above conclusion that such variation of PM_{2.5}-Hg isotope ratios was not controlled by variation of Hg emission sources. The highly positive $\Delta^{199}\text{Hg}$ values observed for daytime samples within the Sun subset (Fig. S2) further supports the conclusion that PM_{2.5}-Hg was strongly affected by photochemical reactions on sunny days.



295

Figure 3. Diel variations of $\Delta^{199}\text{Hg}$ for PM_{2.5}-Hg for the entire dataset, the N-W subset, the S-E subset, and the S-E sunny days only subset. Note that all days included in the N-W subset were sunny. Diel differences within each subset were examined using the Independent Samples T-Test.

300

Linear correlations of $\Delta^{199}\text{Hg}$ versus $\Delta^{201}\text{Hg}$ for all 56 $\text{PM}_{2.5}$ samples (Fig. 4a) and three subsets, N-W (Fig. 4b), S-E (Fig. 4c), and Sun (Fig. 4d), yielded slopes of 1.06 ± 0.05 (1SD, $r^2 = 0.89$), 1.06 ± 0.12 ($r^2 = 0.81$), 1.13 ± 0.05 ($r^2 = 0.92$) and 1.13 ± 0.08 ($r^2 = 0.84$), respectively (Fig. 4). Such slopes are all indicative of photochemical reduction of Hg^{2+} according to prior studies (Bergquist and Blum, 2007; Zheng and Hintelmann, 2009). The photoreduction process is further evidenced by a progressive increase in $\Delta^{199}\text{Hg}$ from zero or slightly negative values to positive values as the content of Hg in $\text{PM}_{2.5}$ (C_{Hg}) decreased in D-samples (Fig. S1a). This trend is statistically more significant ($p < 0.05$) for D-samples within the N-W and Sun subsets (Figs. S1-b and -d). Similarly, for all sunny day samples, a positive correlation ($p < 0.05$) was also observed between $\Delta^{199}\text{Hg}$ and $\delta^{202}\text{Hg}$ (Fig. S3), consistent with prior experimental results (Bergquist and Blum, 2007; Zheng and Hintelmann, 2009). Collectively, the Hg isotope results suggest that photochemical reduction is an important process during the transport of $\text{PM}_{2.5}\text{-Hg}$ in the atmosphere.

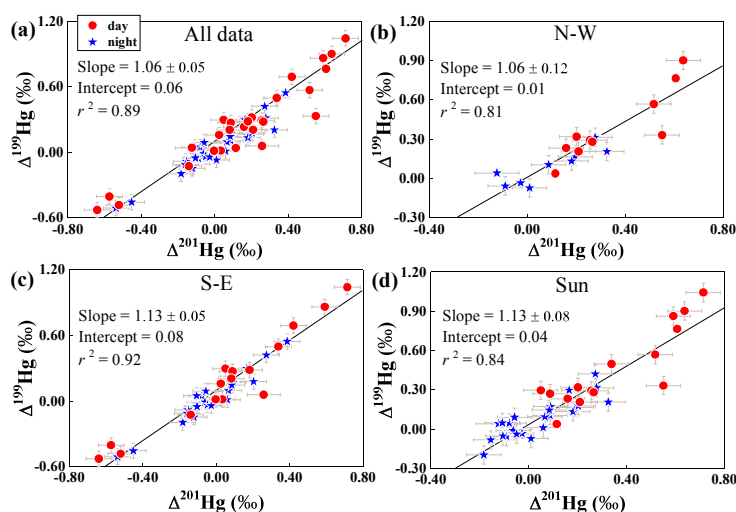


Figure 4. Correlations between $\Delta^{199}\text{Hg}$ and $\Delta^{201}\text{Hg}$ for different subsets of $\text{PM}_{2.5}$ samples: a) all data, b) North-West (N-W), c) South-East (S-E) and d) All sunny days (Sun). The slope, intercept and r -square of the line from simple linear regression. Vertical and horizontal error bars correspond to 2SD analytical precision.

320 Among all D-samples, $\Delta^{199}\text{Hg}$ is only weakly correlated with sunshine duration ($r^2 = 0.20$, p
= 0.02). However, $\Delta^{199}\text{Hg}$ values for all D-samples collected on days with sunshine
durations >8 hrs are positive whereas half of the $\Delta^{199}\text{Hg}$ values for samples collected on cloudy
or hazy days with shorter sunshine durations are negative or near zero (Fig. S4). In addition, a
significant positive linear correlation between $\Delta^{199}\text{Hg}$ values and atmospheric ozone contents
325 (P_{O_3}) ($r^2 = 0.517$, $p < 0.01$) for all but four daytime samples was obtained (Fig. S5). The four
outliners (Sept-16-D, Sept-17-D, Oct-5-D and Oct-6-D) were collected on days with high ozone
(P_{O_3} above 50 ppbv) and severe smog formation. Conversely, no significant correlation ($p >$
0.05) between $\Delta^{199}\text{Hg}$ and P_{O_3} was found for the nighttime samples.

The increase in $\Delta^{199}\text{Hg}$ of daytime $\text{PM}_{2.5}\text{-Hg}$ with sunlight duration and ozone concentration
330 indicates that the physical and photochemical conditions of the atmosphere may affect the
atmospheric transformation of $\text{PM}_{2.5}\text{-Hg}$. A prior experimental study showed that GEM
oxidation can produce negative $\Delta^{199}\text{Hg}$ values in oxidized Hg^{2+} with $\Delta^{199}\text{Hg}/\Delta^{201}\text{Hg}$ ratios of
1.6 and 1.9 for Br and Cl radical initiated oxidations (Sun et al., 2016). We can exclude the
possible contribution of Hg^0 oxidation to $\text{PM}_{2.5}\text{-Hg}$, given the fact that $\Delta^{199}\text{Hg}/\Delta^{201}\text{Hg}$ ratio was
335 about 1.1 and most $\text{PM}_{2.5}\text{-Hg}$ samples collected during the daytime when Br and Cl radicals
could form had positive $\Delta^{199}\text{Hg}$ values. Thus it is highly unlikely that oxidation would have
caused the diel variation in Hg isotopes in $\text{PM}_{2.5}$. However, the exception to the observed
relationships between $\Delta^{199}\text{Hg}$ with sunlight duration, and ozone concentration show that in a
highly oxidizing atmosphere (higher P_{O_3}) such as occurs during extreme smog events, the odd-
340 MIF of Hg isotopes in $\text{PM}_{2.5}$ may decrease or reverse. A possible explanation for this effect
may be the increased production of GOM and its collection with $\text{PM}_{2.5}\text{-Hg}$ during such smog
events. While $\text{PM}_{2.5}\text{-Hg}$ samples collected on quartz fiber filters may include some GOM
(Lynam and Keeler, 2002), this contribution was likely small in most of our D and N samples
due to the opposing diel trends in the concentrations of PBM and GOM in urban air (Engle et

345 al., 2010). GOM would therefore not have had a major effect on the observed diel variations of $\Delta^{199}\text{Hg}$ values for $\text{PM}_{2.5}\text{-Hg}$ and may have in fact masked an even larger MIF signature due to the photoreduction of PBM during the day.

350 Interestingly, negative $\Delta^{199}\text{Hg}$ values in daytime $\text{PM}_{2.5}\text{-Hg}$ were only observed during a rainy day and an extreme smog event. Since the Hg emitted from local sources had close to zero and negative values of odd-MIF, higher humidity (such as during rainy days) and heavy pollution (the extreme smog) may enhance the effect of ~~Seavenging~~ scavenging of locally produced gaseous or particulate HgGOM during rain or smog events, which may therefore have contributed to the reversal of the odd-MIF signature of Hg collected as $\text{PM}_{2.5}$ at these times. In addition, the negative $\Delta^{199}\text{Hg}$ values in $\text{PM}_{2.5}$ may have resulted from the contribution of 355 biomass burning with limited photoreduction effect during periods of less sunshine (Fig. 2 and Table S1) since plant foliage has negative $\Delta^{199}\text{Hg}$ values (Yu et al., 2016) and more negative $\Delta^{199}\text{Hg}$ values (down to -0.53‰) of $\text{PM}_{2.5}\text{-Hg}$ in Beijing were related to biomass burning, a source of $\text{PM}_{2.5}\text{-Hg}$ south of Beijing in autumn (Huang et al., 2016). This could further explain the relatively lower $\Delta^{199}\text{Hg}$ values in the majority of the N-samples (for example, Sept-28-N and Oct-5-N with $\Delta^{199}\text{Hg}$ of -0.46‰ and -0.51‰), even in those collected under clear 360 weathering condition. Indeed, each bulk sample collected during night time was a mixture of the leftover $\text{PM}_{2.5}$ (with positive odd-MIF) from the previous daytime and the $\text{PM}_{2.5}$ newly input from various sources including industrial emissions (with close to zero $\Delta^{199}\text{Hg}$) and biomass burning (somewhat negative $\Delta^{199}\text{Hg}$) (Huang et al., 2016) during nighttime.

365 A possible explanation of the observed effects of diel variation of $\text{PM}_{2.5}\text{-Hg}$ would be the temperature-dependent gas-aerosol partitioning of GOM (Rutter and Schauer, 2007; Amos et al., 2012), which favors more adsorption of GOM on PM during nighttime when atmospheric temperature is relatively lower than daytime. However, the magnitude of such adsorption is also proportional to the GOM concentration in the atmosphere. An inverse calculation exercise

370 (in SI) shows that the higher PM_{2.5}-Hg measured for our samples would require higher GOM
concentrations during the nighttime, which contradicts with prior findings that GOM
concentrations are significantly lower during the nighttime than the daytime as GOM is a
product of photo-oxidation processes (Poissant et al., 2005; Liu et al., 2007; Amos et al., 2012).
In addition, GOM gas-aerosol partitioning is considered a chemisorption and desorption
375 process (Rutter and Schauer, 2007), which unlikely result in appreciable odd-MIF of Hg
isotopes (Jiskra et al., 2012; Smith et al., 2015). Therefore, GOM partitioning would have little
or no effect on the observed diel variations of $\Delta^{199}\text{Hg}$ values for PM_{2.5}-Hg.

Variation in atmosphere boundary layer height (ABLH) from 1000 to 1300 m during daytime
to less than 200 to 300 m during nighttime may have contributed to the diel variation in Hg
380 isotopic composition of PM_{2.5}-Hg (Quan et al., 2013). With a high ABLH during daytime,
relatively strong turbulence may help mixing the PM_{2.5}-Hg from the surface to the upper free
troposphere, where photoreactions may be favored due to higher intensities of ultraviolet
radiation on clear days. In contrast, a lower ABLH at night may weaken the vertical transport
of PM_{2.5}-Hg, but enhance the contribution from newly produced PM_{2.5}-Hg, possibly resulting
385 in higher concentrations of PM_{2.5}-Hg with negative or close to zero $\Delta^{199}\text{Hg}$ values from
emission sources and/or GOM. However, vertically-resolved, day-night measurements of Hg
stable isotope ratios in PBM and GOM are needed to fully evaluate the effects of various
physical processes on diel variation of the Hg isotopic compositions for the PM_{2.5}.

While our results cannot exclude the effects of other possible processes, such as oxidation,
390 adsorption (and desorption)/gas-aerosol partitioning, and precipitation, based on the limited
previous studies (Jiskra et al., 2012; Smith et al., 2015; Sun et al., 2016), these processes are
not likely to be important to the diel variation of odd-MIF of Hg isotopes in PM_{2.5}-Hg we
observed.

3.4 Photochemical reduction as a cause of diel variation in odd-MIF in day-night sample pairs of PM_{2.5}

395

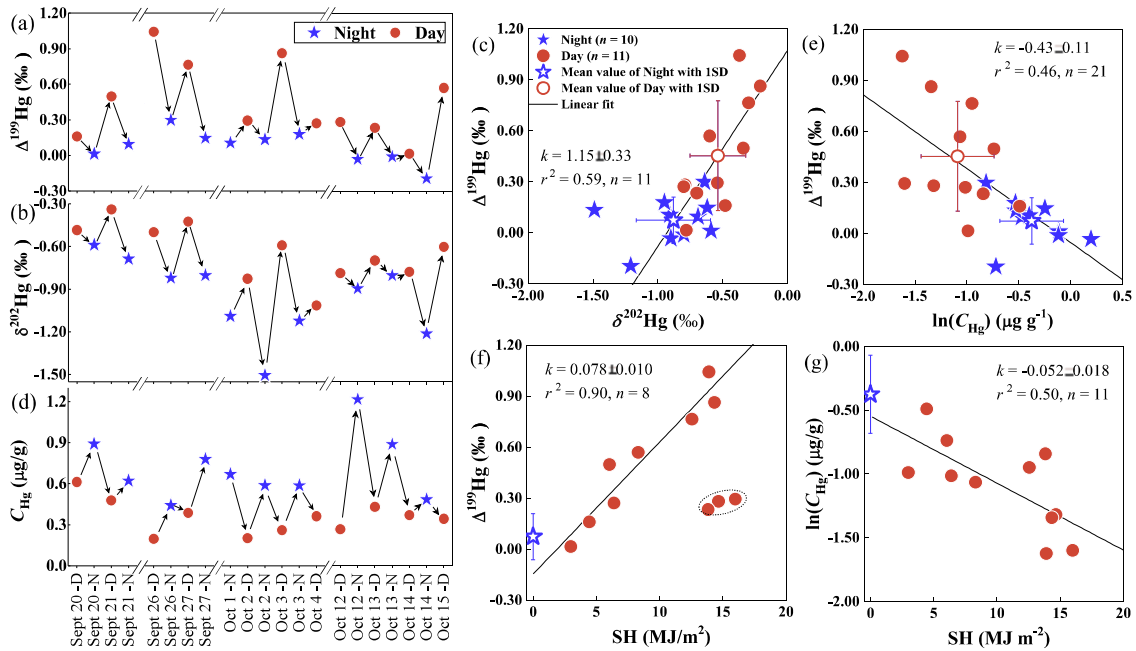
400

405

410

415

To explore the possible causes of diel variation in odd-MIF of Beijing PM_{2.5}-Hg further, we examined four subgroups of PM_{2.5} samples, each of which included 2 to 4 consecutive pairs of D-N samples that were collected during time periods of relatively constant atmospheric conditions (i.e., not being hazy, rainy or windy or having extremely high ozone (P_{O_3} above 50 ppbv)). Within each of the four subgroups, $\Delta^{199}\text{Hg}$ and $\delta^{202}\text{Hg}$ values were lower at night than during the previous or following day (Figs. 5-a and -b). As shown in Figure 5c, there is a significant positive correlation ($p < 0.01$) between $\Delta^{199}\text{Hg}$ and $\delta^{202}\text{Hg}$ values for all samples in these four subgroups, with average values for both day and night falling right on the best fit line. The slope of this line is 1.15 ± 0.33 , which is consistent with the reported value of 1.15 ± 0.07 for photochemical reduction of Hg^{2+} in aqueous solution (Bergquist and Blum, 2007). Coincidentally, the contents of Hg in PM_{2.5} (C_{Hg}) were higher in N-samples than in immediately preceding or following D-samples (Fig. 5d), indicating a negative linear relationship between $\Delta^{199}\text{Hg}$ values and C_{Hg} (Fig. 5e). Moreover, eight of the total eleven daytime samples among the four subgroups showed a positive linear correlation between $\Delta^{199}\text{Hg}$ and the total cumulative daily solar radiation on a horizontal surface (SH) (Fig. 5f). These eleven samples also showed a negative correlation between the logarithmic values of C_{Hg} and SH (Fig. 5g). These correlations are consistent with the photochemical reduction of divalent Hg observed under laboratory conditions, and thus strongly support the hypothesis that photochemical reduction is an important process controlling the fate of ambient atmospheric PM_{2.5}-Hg. Given its diel trend and relatively large range, the MIF of odd Hg isotopes in Beijing PM_{2.5} we observed was most likely due to the magnetic isotope effect (MIE), which has been invoked to explain MIF during the photochemical reduction of aqueous Hg^{2+} (Zheng and Hintelmann, 2010b).



420 **Figure 5.** Hg isotope ratios and contents in four subgroups of consecutive pairs of day-night samples collected during periods of relatively constant atmospheric conditions. Linear correlations between $\Delta^{199}\text{Hg}$ and $\delta^{202}\text{Hg}$ (c), C_{Hg} (e) and the total cumulative daily solar radiation on a horizontal surface (SH, MJ m^{-2}) (f), and between C_{Hg} and SH (g) were displayed

425 The uncertainty for measurement of $\Delta^{199}\text{Hg}$ and $\delta^{202}\text{Hg}$ of $\text{PM}_{2.5}$ samples were 0.06‰ and 0.12‰ in 2SD, respectively.

3.5 Even isotope MIF

Diel variation of $\Delta^{200}\text{Hg}$ signatures was also observed in $\text{PM}_{2.5}\text{-Hg}$. Prior studies reported mainly positive $\Delta^{200}\text{Hg}$ values for wet precipitation (up to 1.24‰) (Gratz et al., 2010; Chen et al., 2012; Wang et al., 2015; Yuan et al., 2015) and aerosols (-0.05% to 0.28%) (Rolison et al., 2013; Das et al., 2016; Huang et al., 2016). Even Hg isotope MIF has been attributed to complex redox processes occurring in the upper atmosphere, but the underlying mechanisms remain unclear (Mead et al., 2013; Eiler et al., 2014). Thus, the even-MIF signatures may suggest a small proportion of $\text{PM}_{2.5}\text{-Hg}$ is likely originated from the upper atmosphere, through

435 for example long-term transport and/or ABLH increasing during daytime. Given the fact that all samples displayed only slightly positive $\Delta^{200}\text{Hg}$ (average $0.07\% \pm 0.06\%$, 1SD), this

contribution may be very limited. In addition, $\Delta^{200}\text{Hg}$ values are weakly, but significantly correlated with $\Delta^{199}\text{Hg}$ ($r^2 = 0.13, p < 0.01$) (Fig. S6) and $\delta^{202}\text{Hg}$ ($r^2 = 0.27, p < 0.01$) (Fig. S7). No mechanistic explanation is available yet for such observations, however.

440

4 Conclusions

This study showed significant diel variations of Hg isotopic compositions for ambient $\text{PM}_{2.5}\text{-Hg}$ collected in the city of Beijing. The Hg isotope signatures featured a large range of MDF ($\delta^{202}\text{Hg}$ value from -1.49‰ to 0.55‰ , mean of $-0.53\text{‰} \pm 0.40\text{‰}$) and significant ($p < 0.05$) MIF with more positive $\Delta^{199}\text{Hg}$ values in daytime samples ($0.26\text{‰} \pm 0.40\text{‰}$) than at night ($0.04\text{‰} \pm 0.22\text{‰}$). The results clearly indicated that the Hg isotope compositions of $\text{PM}_{2.5}\text{-Hg}$ are impacted variously by both weather conditions (such as sunlight duration), which may promote the photochemical reaction, and directions of air mass trajectories, which are related to possible sources of $\text{PM}_{2.5}$. D-N paired samples having similar air mass backward trajectories and hence similar sources exhibited strong positive correlations between $\Delta^{199}\text{Hg}$ and $\Delta^{201}\text{Hg}$ with a slope of 1.1 and $\Delta^{199}\text{Hg}$ and $\delta^{202}\text{Hg}$ with a slope of 1.15, and a decrease in the content of Hg in $\text{PM}_{2.5}$ as $\Delta^{199}\text{Hg}$ increased. These results provide isotopic evidence that local, daytime photochemical reduction of divalent Hg is of critical importance to the fate of $\text{PM}_{2.5}\text{-Hg}$ in urban atmosphere. Although the specific reactions and mechanisms that control Hg isotope fractionation (MDF and MIF) in Beijing $\text{PM}_{2.5}$ could not be explicitly determined from this field study, our result illustrated that, in addition to variation in sources, photochemical reduction appears to be an important process that affects both the content and isotopic composition of $\text{PM}_{2.5}\text{-Hg}$. Further systematic study is thus needed to better quantify the photoreduction of $\text{PM}_{2.5}\text{-Hg}$ to estimate the percentage of reduced Hg it produces and its impact on the global biogeochemical cycling of Hg.

445
450
455
460

Acknowledgments. We thank the anonymous reviewers for their constructive comments and suggestions. This study was supported financially by the National Key Research and Development Program of China (No. 2017YFC0212702), Natural Science Foundation of China (no. 41701268, 41625012, 41273023), Guizhou Scientific Research Program (No. 20161158) and State Key Laboratory of Organic Geochemistry (OGL-201501).

References

- Amos, H. M., Jacob, D. J., Holmes, C. D., Fisher, J. A., Wang, Q., Yantosca, R. M., Corbitt, E. S., Galarneau, E., Rutter, A. P., Gustin, M. S., Steffen, A., Schauer, J. J., Graydon, J. A., St Louis, V. L., Talbot, R. W., Edgerton, E. S., Zhang, Y., and Sunderland, E. M.: Gas-particle partitioning of atmospheric Hg(II) and its effect on global mercury deposition, *Atmos. Chem. Phys.*, 12, 591-603, 2012.
- Bergquist, B. A., and Blum, J. D.: Mass-dependent and -independent fractionation of Hg isotopes by photoreduction in aquatic systems, *Science*, 318, 417-420, 2007.
- Blum, J. D., and Bergquist, B. A.: Reporting of variations in the natural isotopic composition of mercury, *Anal. Bioanal. Chem.*, 388, 353-359, 2007.
- Cai, H., and Chen, J.: Mass-independent fractionation of even mercury isotopes, *Science Bulletin*, 61, 116-124, 10.1007/s11434-015-0968-8, 2016.
- Chen, J. B., Hintelmann, H., and Dimock, B.: Chromatographic pre-concentration of Hg from dilute aqueous solutions for isotopic measurement by MC-ICP-MS, *J. Anal. At. Spectrom.*, 25, 1402-1409, 2010.
- Chen, J. B., Hintelmann, H., Feng, X. B., and Dimock, B.: Unusual fractionation of both odd and even mercury isotopes in precipitation from Peterborough, ON, Canada, *Geochim. Cosmochim. Acta*, 90, 33-46, 2012.
- Das, R., Wang, X., Khezri, B., Webster, R. D., Sikdar, P. K., and Datta, S.: Mercury isotopes of atmospheric particle bound mercury for source apportionment study in urban Kolkata, India, *Elementa: Science of the Anthropocene*, 4, 000098, 2016.

- Eiler, J. M., Bergquist, B., Bourg, I., Cartigny, P., Farquhar, J., Gagnon, A., Guo, W., Halevy, I., Hofmann, A., Larson, T. E., Levin, N., Schauble, E. A., and Stolper, D.: Frontiers of stable isotope geoscience, *Chem. Geol.*, 372, 119-143, 2014.
- Engle, M. A., Tate, M. T., Krabbenhoft, D. P., Schauer, J. J., Kolker, A., Shanley, J. B., and Bothner, M. H.: Comparison of atmospheric mercury speciation and deposition at nine sites across central and eastern North America, *J. Geophys. Res. Atmos.*, 115, 2010.
- Estrade, N., Carignan, J., Sonke, J. E., and Donard, O. F. X.: Mercury isotope fractionation during liquid-vapor evaporation experiments, *Geochim. Cosmochim. Acta*, 73, 2693-2711, 2009.
- Ghosh, S., Schauble, E. A., Lacrampe Couloume, G., Blum, J. D., and Bergquist, B. A.: Estimation of nuclear volume dependent fractionation of mercury isotopes in equilibrium liquid–vapor evaporation experiments, *Chem. Geol.*, 336, 5-12, 2013.
- Gratz, L. E., Keeler, G. J., Blum, J. D., and Sherman, L. S.: Isotopic composition and fractionation of mercury in Great Lakes precipitation and ambient air, *Environ. Sci. Technol.*, 44, 7764-7770, 2010.
- Hintelmann, H., and Lu, S. Y.: High precision isotope ratio measurements of mercury isotopes in cinnabar ores using multi-collector inductively coupled plasma mass spectrometry, *Analyst*, 128, 635-639, 2003.
- Huang, Q., Liu, Y. L., Chen, J. B., Feng, X. B., Huang, W. L., Yuan, S. L., Cai, H. M., and Fu, X. W.: An improved dual-stage protocol to pre-concentrate mercury from airborne particles for precise isotopic measurement, *J. Anal. At. Spectrom.*, 30, 957-966, 2015.
- Huang, Q., Chen, J., Huang, W., Fu, P., Guinot, B., Feng, X., Shang, L., Wang, Z., Wang, Z., Yuan, S., Cai, H., Wei, L., and Yu, B.: Isotopic composition for source identification of mercury in atmospheric fine particles, *Atmos. Chem. Phys.*, 16, 11773-11786, 2016.
- Jackson, T. A., Muir, D. C. G., and Vincent, W. F.: Historical variations in the stable isotope composition of mercury in Arctic Lake sediments, *Environ. Sci. Technol.*, 38, 2813-2821, 2004.
- Jackson, T. A., Whittle, D. M., Evans, M. S., and Muir, D. C. G.: Evidence for mass-independent and mass-dependent fractionation of the stable isotopes of mercury by natural processes in aquatic ecosystems, *Appl. Geochem.*, 23, 547-571, 2008.

- Janssen, S. E., Schaefer, J. K., Barkay, T., and Reinfelder, J. R.: Fractionation of mercury stable isotopes during microbial methylmercury production by iron- and sulfate-reducing bacteria, Environ. Sci. Technol., 50, 8077-8083, 2016.
- Jiskra, M., Wiederhold, J. G., Bourdon, B., and Kretzschmar, R.: Solution speciation controls mercury isotope fractionation of Hg(II) sorption to goethite, Environ. Sci. Technol., 46, 6654-6662, 2012.
- Kritee, K., Blum, J. D., Johnson, M. W., Bergquist, B. A., and Barkay, T.: Mercury stable isotope fractionation during reduction of Hg(II) to Hg(0) by mercury resistant microorganisms, Environ. Sci. Technol., 41, 1889-1895, 2007.
- Liu, B., Keeler, G. J., Dvonch, J. T., Barres, J. A., Lynam, M. M., Marsik, F. J., and Morgan, J. T.: Temporal variability of mercury speciation in urban air, Atmos. Environ., 41, 1911-1923, 2007.
- Lynam, M. M., and Keeler, G. J.: Comparison of methods for particulate phase mercury analysis: Sampling and analysis, Anal. Bioanal. Chem., 374, 1009-1014, 2002.
- Mead, C., Lyons, J. R., Johnson, T. M., and Anbar, A. D.: Unique Hg stable isotope signatures of compact fluorescent lamp-sourced Hg, Environ. Sci. Technol., 47, 2542-2547, 2013.
- Poissant, L., Pilote, M., Beauvais, C., Constant, P., and Zhang, H. H.: A year of continuous measurements of three atmospheric mercury species (GEM, RGM and Hg-p) in southern Quebec, Canada, Atmos. Environ., 39, 1275-1287, 2005.
- Quan, J. N., Gao, Y., Zhang, Q., Tie, X. X., Cao, J. J., Han, S. Q., Meng, J. W., Chen, P. F., and Zhao, D. L.: Evolution of planetary boundary layer under different weather conditions, and its impact on aerosol concentrations, Particuology, 11, 34-40, 2013.
- Rolison, J. M., Landing, W. M., Luke, W., Cohen, M., and Salters, V. J. M.: Isotopic composition of species-specific atmospheric Hg in a coastal environment, Chem. Geol., 336, 37-49, 2013.
- Rose, C. H., Ghosh, S., Blum, J. D., and Bergquist, B. A.: Effects of ultraviolet radiation on mercury isotope fractionation during photo-reduction for inorganic and organic mercury species, Chem. Geol., 405, 102-111, 2015.
- Rutter, A. P., and Schauer, J. J.: The effect of temperature on the gas-particle partitioning of reactive mercury in atmospheric aerosols, Atmos. Environ., 41, 8647-8657, 2007.

- Schleicher, N. J., Schäfer, J., Blanc, G., Chen, Y., Chai, F., Cen, K., and Norra, S.: Atmospheric
550 particulate mercury in the megacity Beijing: Spatio-temporal variations and source
apportionment, *Atmos. Environ.*, 109, 251-261, 2015.
- Selin, N. E.: Global biogeochemical cycling of mercury: A review, *Annu. Rev. Env. Resour.*,
34, 43-63, 2009.
- Sherman, L. S., Blum, J. D., Johnson, K. P., Keeler, G. J., Barres, J. A., and Douglas, T. A.:
555 Mass-independent fractionation of mercury isotopes in Arctic snow driven by sunlight,
Nature Geosci., 3, 173-177, 2010.
- Sherman, L. S., Blum, J. D., Keeler, G. J., Demers, J. D., and Dvornch, J. T.: Investigation of
local mercury deposition from a coal-fired power plant using mercury isotopes, *Environ. Sci.
Technol.*, 46, 382-390, 2012.
- 560 Smith, R. S., Wiederhold, J. G., and Kretzschmar, R.: Mercury isotope fractionation during
precipitation of metacinnabar (β -HgS) and montroydite (HgO), *Environ. Sci. Technol.*, 49,
4325-4334, 2015.
- Subir, M., Ariya, P. A., and Dastoor, A. P.: A review of the sources of uncertainties in
atmospheric mercury modeling II. Mercury surface and heterogeneous chemistry—A missing
565 link, *Atmos. Environ.*, 46, 1-10, 2012.
- Sun, G., Sommar, J., Feng, X., Lin, C.-J., Ge, M., Wang, W., Yin, R., Fu, X., and Shang, L.:
Mass-dependent and -independent fractionation of mercury isotope during gas-phase
oxidation of elemental mercury vapor by atomic Cl and Br, *Environ. Sci. Technol.*, 50, 9232-
9241, 2016.
- 570 Wang, Z., Chen, J., Feng, X., Hintelmann, H., Yuan, S., Cai, H., Huang, Q., Wang, S., and
Wang, F.: Mass-dependent and mass-independent fractionation of mercury isotopes in
precipitation from Guiyang, SW China, *C. R. Geosci.*, 347, 358-367, 2015.
- Wiederhold, J. G., Cramer, C. J., Daniel, K., Infante, I., Bourdon, B., and Kretzschmar, R.:
Equilibrium mercury isotope fractionation between dissolved Hg(II) species and thiol-bound
575 Hg, *Environ. Sci. Technol.*, 44, 4191-4197, 2010.
- Xu, H., Sonke, J. E., Guinot, B., Fu, X., Sun, R., Lanzasova, A., Candaudap, F., Shen, Z., and
Cao, J.: Seasonal and annual variations in atmospheric Hg and Pb isotopes in Xi'an, China,
Environ. Sci. Technol., 51, 3759-3766, 2017.

- Yang, L., and Sturgeon, R.: Isotopic fractionation of mercury induced by reduction and
580 ethylation, *Anal. Bioanal. Chem.*, 393, 377-385, 2009.
- Yu, B., Fu, X., Yin, R., Zhang, H., Wang, X., Lin, C.-J., Wu, C., Zhang, Y., He, N., Fu, P.,
Wang, Z., Shang, L., Sommar, J., Sonke, J. E., Maurice, L., Guinot, B., and Feng, X.: Isotopic
composition of atmospheric mercury in China: New evidence for sources and transformation
processes in air and in vegetation, *Environ. Sci. Technol.*, 50, 9262-9269, 2016.
- 585 Yuan, S., Zhang, Y., Chen, J., Kang, S., Zhang, J., Feng, X., Cai, H., Wang, Z., Wang, Z., and
Huang, Q.: Large variation of mercury isotope composition during a single precipitation
event at Lhasa city, Tibetan Plateau, China, *Procedia Earth and Planetary Science*, 13, 282-
286, 2015.
- Zhang, L., Wang, S. X., Wang, L., Wu, Y., Duan, L., Wu, Q. R., Wang, F. Y., Yang, M., Yang,
590 H., Hao, J. M., and Liu, X.: Updated emission inventories for speciated atmospheric mercury
from anthropogenic sources in China, *Environ. Sci. Technol.*, 49, 3185-3194, 2015.
- Zhang, Q., Jimenez, J. L., Canagaratna, M. R., Allan, J. D., Coe, H., Ulbrich, I., Alfarra, M. R.,
Takami, A., Middlebrook, A. M., Sun, Y. L., Dzepina, K., Dunlea, E., Docherty, K., DeCarlo,
P. F., Salcedo, D., Onasch, T., Jayne, J. T., Miyoshi, T., Shimojo, A., Hatakeyama, S.,
595 Takegawa, N., Kondo, Y., Schneider, J., Drewnick, F., Borrmann, S., Weimer, S., Demerjian,
K., Williams, P., Bower, K., Bahreini, R., Cottrell, L., Griffin, R. J., Rautiainen, J., Sun, J.
Y., Zhang, Y. M., and Worsnop, D. R.: Ubiquity and dominance of oxygenated species in
organic aerosols in anthropogenically-influenced Northern Hemisphere midlatitudes,
Geophys. Res. Lett., 34, 2007.
- 600 Zheng, W., and Hintelmann, H.: Mercury isotope fractionation during photoreduction in natural
water is controlled by its Hg/DOC ratio, *Geochim. Cosmochim. Acta*, 73, 6704-6715, 2009.
- Zheng, W., and Hintelmann, H.: Nuclear field shift effect in isotope fractionation of mercury
during abiotic reduction in the absence of light, *J. Phys. Chem. A*, 114, 4238-4245, 2010a.
- Zheng, W., and Hintelmann, H.: Isotope fractionation of mercury during its photochemical
605 reduction by low-molecular-weight organic compounds, *J. Phys. Chem. A*, 114, 4246-4253,
2010b.

Supporting Information

Diel variation of mercury stable isotope ratios record photoreduction of PM_{2.5}-bound

mercury

5 Qiang Huang^{1,2}, Jiubin Chen^{1,3,*}, Weilin Huang⁴, John R. Reinfelder⁴, Pingqing Fu⁵, Shengliu Yuan¹, Zhongwei Wang¹, Wei Yuan¹, Hongming Cai¹, Hong Ren⁵, Yele Sun⁵ and Li He⁶

¹ SKLEG, Institute of Geochemistry, CAS, Guiyang 550081, China

² SKLOG, Guangzhou Institute of Geochemistry, CAS, Guangzhou 510640, China

10 ³ Institute of Surface-Earth System Science, Tianjin University, 300072, China

⁴ Department of Environmental Sciences, Rutgers, The State University of New Jersey, New Brunswick, NJ 08901, USA

⁵ LAPC, Institute of Atmospheric Physics, CAS, Beijing 100029, China

15 ⁶ Laboratory of Hebei Institute of Regional Geology and Mineral Resources Survey, Shijiazhuang 065000, China

*Corresponding author.

E-mail: jbchen@tju.edu.cn

20	Page S2	Materials and methods
	Page S7	Table S1
	Page S8	Table S2
	Page S9	Table S3
	Page S10	Table S4
25	Page S11	Figure S1
	Page S15	Figure S2
	Page S16	Figure S3
	Page S17	Figure S4
	Page S18	Figure S5
30	Page S19	Figure S6
	Page S20	Figure S7
	Page S21	References

1. Materials and methods

1.1 Materials

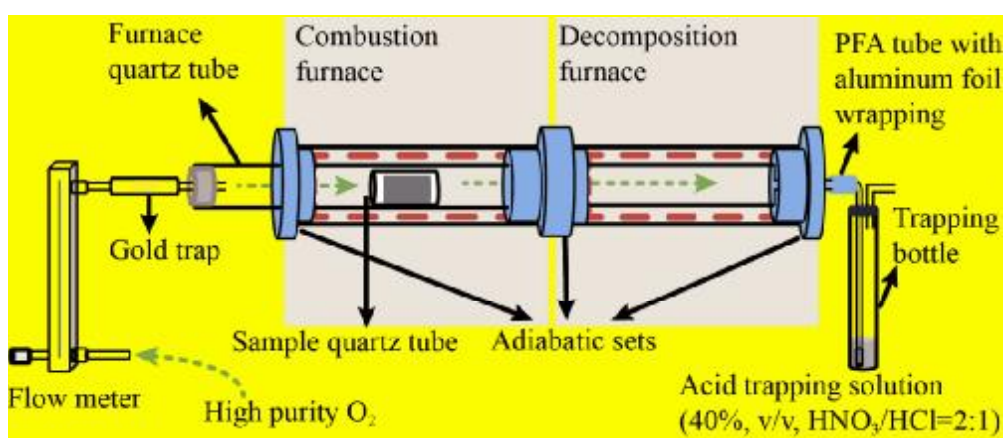
35 HCl, HNO₃ and stannous chloride (SnCl₂) were analytical grade (Sinopharm Chemical Reagent Co., Ltd., China). Milli-Q water (18.2 MΩ, Millipore, USA) was used for preparation all aqueous solutions. Concentrated HCl and HNO₃ were double-distilled using a DST-1000 acid purification system (Savillex, USA). Two SnCl₂ solutions of 0.20 and 0.03 g/mL were prepared by dissolving the solid SnCl₂ in 1 M HCl and were used for online reduction of Hg²⁺
40 during the content and isotope measurements, respectively. The National Institute of Standards and Technology Standard Reference Material 3133 (NIST SRM 3133) Hg and UM-Almaden Hg were used as international standards and measured regularly to control the accuracy and quality of isotope analysis. Two other reference materials, the solution NIST SRM 3177 Hg and the Yellow-Red Soil GBW07405 (National Center for Standard Materials, Beijing, China)
45 were used as in-house isotope standards, and were regularly measured for quality control of Hg content and isotope measurements. GBW07405 was also used as procedure standard to evaluate the accuracy and precision of sample pretreatment (Huang et al., 2015; Huang et al., 2016). The NIST SRM 997 Thallium (20 ng mL⁻¹ Tl in 3 % HNO₃) was employed as an internal standard for mass bias correction.

50

1.2 Sample pretreatment for mercury isotopes analysis

After collection, mercury bound on PM_{2.5} with sufficient mass for isotopic analysis (≥ 10 ng) was concentrated into a 5-mL 40% acid mixture (2:4:9 volumetric ratio of 10 M HCl, 15 M HNO₃ and Milli-Q water) according to the methods reported in Huang et al. (2015). Schematic
55 diagram of the combustion-trapping assembly from Huang et al. (2015) is shown below. To

extract Hg bound to PM samples, each filter was rolled into a cylinder and placed in a sample quartz tube. Both ends of the tube were capped with quartz wool (pre-cleaned at 500°C) to prevent particle emission. Each tube was combusted over 2 h in a temperature-programmed dual-stage quartz tube combustion furnace in which the temperature of the first furnace was incrementally increased to 900°C whereas the second furnace was held at 950°C. The resulting Hg vapor was swept by O₂ gas (Hg free) into the 40% acid trapping solution. The trapping solution was diluted with Milli-Q H₂O to 10 mL to a final acid concentration of 20%. The accuracy and precision of the dual-stage combustion protocol were evaluated by the analysis of the GBW07405 using the same digestion method. The detection limit given by the procedural blanks (< 0.3 ng) for this dual-stage combustion method was negligibly low compared to the total Hg mass (≥ 10 ng) extracted from either PM_{2.5} samples or procedural standards.



Schematic diagram of the combustion-trapping assembly from Huang et al. (2015).

70 1.3 Mercury concentration and stable isotope composition measurements

The methods used to measure the Hg content and isotope ratio were published elsewhere (Huang et al., 2015). In brief, a small fraction of each trapping solution (20% acid mixture) was used to measure the Hg content on cold-vapor atomic fluorescence spectroscopy (CVAFS,

Tekran 2500, Tekran® Instruments Corporation, CA), with a precision better than 10%. The
75 recoveries of Hg for the standard GBW07405 were in the acceptable range of 95 to 105% with
an average value of 98% (1 SD = 6%, $n = 6$); but no recovery of Hg for the PM_{2.5} samples was
determined due to limited availability of the samples.

A total of 61 PM_{2.5} samples were collected during the sampling campaign. After analysis
of Hg contents, we found that 56 PM_{2.5} samples (including 26 daytime and 30 nighttime samples)
80 have sufficient Hg mass and hence were further analyzed for Hg isotope compositions using a
multicollector inductively coupled plasma mass spectrometer (MC-ICP-MS, Nu Instruments
Ltd., UK) equipped with a continuous flow cold vapor generation system. Detailed protocols
for the Hg isotope analysis can be found in Huang et al. (2015). The Faraday cups were
positioned to simultaneously collect five Hg isotopes and two Tl isotopes including ²⁰⁵Tl (H3),
85 ²⁰³Tl (H1), ²⁰²Hg (Ax), ²⁰¹Hg (L1), ²⁰⁰Hg (L2), ¹⁹⁹Hg (L3), and ¹⁹⁸Hg (L4). ¹⁹⁶Hg and ²⁰⁴Hg
were not measured due to their very low abundance. Instrumental mass bias was corrected using
an internal standard (NIST SRM 997 Tl) and strict sample-standard bracketing with NIST SRM
3133 Hg standard. For quality assurance and control, the well-known reference material UM-
Almaden and the NIST SRM 3177 Hg were inserted repeatedly into the sampling list after every
90 ten and five real samples, measured regularly during sample analysis session, and calibrated
periodically against the NIST SRM 3133 Hg as well as samples.

Delta (δ) notation is used to represent MDF in units of per mil (‰) as defined by the
following equation (Blum and Bergquist, 2007):

$$\delta^x\text{Hg} (\text{‰}) = [({}^x\text{Hg}/{}^{198}\text{Hg})_{\text{sample}}/({}^x\text{Hg}/{}^{198}\text{Hg})_{\text{NIST3133}} - 1] \times 1000 \quad (1)$$

95 where $x = 199, 200, 201,$ and 202 . MIF is reported as the deviation of a measured delta value
from the theoretically predicted MDF value according to the equation:

$$\Delta^x\text{Hg} (\%) = \delta^x\text{Hg} - \beta \times \delta^{202}\text{Hg} \quad (2)$$

where the mass-dependent scaling factor β is 0.252, 0.5024, and 0.752 for ^{199}Hg , ^{200}Hg and ^{201}Hg , respectively (Blum and Bergquist, 2007).

100

1.4 Backward trajectory analysis

The backward HYSPLIT trajectories of air masses at a height of 500 m above ground level and arriving at the sampling site (at 39.9725 N 116.3683 E) were simulated. Because the average boundary layer heights was reported about 500 m in Beijing (Xiang et al., 2019), so the arrival height of 500 m used for backward HYSPLIT trajectories of air masses could be acceptable in this study. In fact, different arrival heights (200, 500, 1000 m AGL) of backward trajectories were tested and results indicated that the transport pathways were not very sensitive to the selected heights within the studied area. Backward trajectories for each sample, ending at 1100 UTC (equal to local time 7:00 p.m.) for daytime sample and ending at 2300 UTC (equal to local time 7:00 a.m.) for nighttime sample, were calculated every 1 hrs using the Internet-Based HYSPLIT Trajectory Model and gridded meteorological data (Global Data Assimilation System, GDAS1) from the U.S. National Oceanic and Atmospheric Administration (NOAA) and were shown below (Fig. S1). The obtained average directions of arriving air masses for each sample were summarized in Table S1. The frequencies of backward trajectories were also calculated for all the samples taken during Sept. 15th to Oct. 16th 2015 using the Internet-Based HYSPLIT Trajectory Model and the archived GDAS0p5, with an interval of 3 hrs, each trajectory total run time 72 hrs and a 0.5×0.5 degree trajectory frequency grid resolution. The results of such simulation showed the dominating air mass arriving from southwest of the sampling site (see Fig. 1).

120 1.5 GOM calculation

We used an inverse approach and a GOM partitioning model to compute hypothetical GOM levels corresponding to each of our PBM observations at ambient temperature. We used the GOM gas-aerosol partitioning model proposed by Amos et al. (2012), which has the following equation: $\log_{10}(K^{-1}) = (10 \pm 1) - (2500 \pm 300)/T$, where $K = (\text{PBM}/\text{PM}_{2.5})/\text{GOM}$ with PBM and GOM in common volumetric units (pg m^{-3}), $\text{PM}_{2.5}$ in $\mu\text{g m}^{-3}$, and T in K. We used the measured $\text{PM}_{2.5}\text{-Hg}$ as PBM and assumed that the $\text{PM}_{2.5}\text{-Hg}$ measured for each sample is 100% in divalent and active mercury forms. The calculated GOM concentrations are presented in the following Table S4. In summary, the calculated GOM concentrations range from 1.5 to 31 pg m^{-3} , with average values of $11 \pm 5 \text{ pg m}^{-3}$ during the daytime and $13 \pm 7 \text{ pg m}^{-3}$ during the nighttime. Overall, the calculated GOM exhibit insignificant ($p = 0.195$, paired samples t -test) diel variation of GOM concentration, i.e., there would be little or no difference of GOM between day- and night-time. Close inspection of the data (Table S4) showed that half of the paired day-night samples have higher calculated GOM concentrations during the nighttime than in daytime.

135 **Table S1.** List of 61 PM_{2.5} samples and their associated weather data.

Name	Sampling date	Start time	End time	Directions of arriving air mass	Weather	Sunshine duration (hrs)	SH (MJ/m ²)	O ₃ (ppbv)	T (°C)	RH (%)	MWS (m/s)	WS (m/s)
Sept-15-N	Sept-15-2015	19:02	7:02	S-SW	Cloudy			7.3	19.8	68	3.9	2
Sept-16-D	Sept-16-2015	8:25	18:55	SW	Sunny	8	6.40	67.7	24.1	52	3.9	2
Sept-16-N	Sept-16-2015	19:02	7:02	SW	Cloudy			5.6	21.1	70	3.9	2
Sept-17-D	Sept-17-2015	8:13	18:43	SW	Cloudy	4	3.02	72.3	24.8	56	4.0	2
Sept-17-N	Sept-17-2015	19:03	7:33	SW-NW	Cloudy+Rain			19.1	22.6	74	4.0	2
Sept-18-D	Sept-18-2015	8:19	18:49	N	Sunny	9	13.24	43.2	27.3	39	3.1	2
Sept-18-N	Sept-18-2015	18:57	7:27	N-NE	Clear			1.1	21.7	54	3.1	2
Sept-19-D	Sept-19-2015	8:07	18:37	NE-E	Sunny	11	17.20	41.5	26.1	33	3.6	1
Sept-19-N	Sept-19-2015	18:48	7:18	S	Clear			4.8	21.7	60	3.6	1
Sept-20-D	Sept-20-2015	8:04	18:34	SW	Cloudy	7	4.45	34.4	24.5	55	4.3	2
Sept-20-N	Sept-20-2015	18:42	7:12	SW	Cloudy			5.7	21.9	62	4.3	2
Sept-21-D	Sept-21-2015	8:17	18:47	SW	Sunny	9	6.04	41.3	25.2	49	4.1	2
Sept-21-N	Sept-21-2015	18:55	7:25	S	Cloudy			18.6	22.6	62	4.1	2
Sept-22-D	Sept-22-2015	8:18	18:18	S-SW	Overcast+Rain	0	0.43	31.4	22.9	70	5.4	2
Sept-22-N	Sept-22-2015	18:28	6:58	W-NW	Cloudy			6.3	18.3	86	5.4	2
Sept-23-D	Sept-23-2015	8:13	18:13	S-NW	Sunny	9	11.20	36.1	23.9	54	2.7	2
Sept-23-N	Sept-23-2015	18:13	6:56	S-SW	Cloudy			3.3	21.6	71	2.7	2
Sept-24-D	Sept-24-2015	8:07	18:07	S	Cloudy	2	0.73	26.5	23.0	72	3.8	2
Sept-24-N	Sept-24-2015	18:15	6:45	SE-W	Cloudy+Rain			19.4	17.7	87	3.8	2
Sept-25-D	Sept-25-2015	8:28	18:28	NW	Sunny	11	18.43	28.6	24.4	19	4.8	2
Sept-25-N	Sept-25-2015	19:03	7:33	SW-NW	Clear			1.2	17.3	44	4.8	2
Sept-26-D	Sept-26-2015	8:06	18:06	SW	Sunny	10	13.90	36.1	23.7	37	5.9	2
Sept-26-N	Sept-26-2015	18:12	6:42	SW-W	Clear			6.2	20.5	59	5.9	2
Sept-27-D	Sept-27-2015	8:21	18:21	N-NE	Sunny	10	12.56	41.9	23.8	42	3.3	2
Sept-27-N	Sept-27-2015	18:38	7:08	N-E	Cloudy			10.2	-	-	3.3	2
Sept-28-D	Sept-28-2015	8:39	18:39	E	Overcast+Rain	0	-	14.1	18.1	82	4.0	2
Sept-28-N	Sept-28-2015	18:47	7:17	E	Overcast+Rain			1.0	17.4	81	4.0	2
Sept-29-D	Sept-29-2015	8:03	18:03	E-SE	Overcast+Rain	0	-	6.7	15.7	88	3.0	2
Sept-29-N	Sept-29-2015	18:33	7:03	SE	Overcast+Rain			0.9	14.7	92	3.0	2
Sept-30-D	Sept-30-2015	8:14	18:14	SW	Cloudy+Rain	3	3.70	19.4	18.1	68	3.2	2
Sept-30-N	Sept-30-2015	18:55	7:25	SW-NW	Cloudy+Rain			13.9	15.5	67	3.2	2
Oct-1-D	Oct-1-2015	7:26	18:31	NW	Sunny	11	17.68	29.2	19.4	27	7.4	3
Oct-1-N	Oct-1-2015	18:41	7:11	NW	Clear			1.7	15.8	51	7.4	3
Oct-2-D	Oct-2-2015	8:50	18:50	NW	Sunny	11	16.00	37.6	24.3	27	4.8	2
Oct-2-N	Oct-2-2015	18:58	7:28	NW	Clear			3.2	18.4	49	4.8	2
Oct-3-D	Oct-3-2015	8:05	18:05	N-S	Sunny	10	14.35	29.1	22.5	35	4.6	2
Oct-3-N	Oct-3-2015	18:30	7:00	SW	Clear			2.1	17.7	66	4.6	2
Oct-4-D	Oct-4-2015	8:20	18:20	SW	Sunny	9	6.40	32.1	21.5	52	2.7	1
Oct-4-N	Oct-4-2015	18:44	7:14	SW	Clear			1.4	17.9	74	2.7	1
Oct-5-D	Oct-5-2015	8:03	18:03	SW	Haze	6	3.89	51.6	21.8	59	3.0	1
Oct-5-N	Oct-5-2015	19:04	7:34	SW	Haze			2.8	18.3	83	3.0	1
Oct-6-D	Oct-6-2015	8:24	18:24	SW-W	Haze	5	3.03	71.4	23.0	60	2.7	1
Oct-6-N	Oct-6-2015	19:25	7:25	SW	Haze			3.4	19.8	81	2.7	1
Oct-7-D	Oct-7-2015	7:55	16:55	SW-NW	Haze	2	1.66	31.6	22.6	68	3.4	2
Oct-7-N	Oct-7-2015	18:00	6:00	NW	Clear			18.9	19.1	24	3.4	2
Oct-8-D	Oct-8-2015	8:07	18:07	NW	Sunny	11	16.11	24.9	17.8	15	7.1	3
Oct-8-N	Oct-8-2015	18:43	6:43	NW	Clear			2.6	14.3	31	7.1	3
Oct-9-D	Oct-9-2015	7:43	17:13	NW	Sunny	11	12.81	18.1	18.7	20	8.3	4
Oct-9-N	Oct-9-2015	17:53	5:23	NW-N	Cloudy			17.9	12.5	30	8.3	4
Oct-10-D	Oct-10-2015	8:10	18:10	NW-N	Sunny	10	12.75	23.8	14.4	24	7.7	4
Oct-10-N	Oct-10-2015	18:38	7:08	N	Cloudy			23.3	15.3	27	7.7	4
Oct-11-D	Oct-11-2015	8:35	18:00	N	Sunny	10	12.63	30.4	20.1	26	7.1	3
Oct-11-N	Oct-11-2015	18:08	6:38	N	Cloudy			5.8	16.6	27	7.1	3
Oct-12-D	Oct-12-2015	7:49	17:31	NW	Sunny	11	14.67	27.4	22.5	20	5.9	1
Oct-12-N	Oct-12-2015	17:40	6:10	NW	Cloudy			2.7	17.8	34	5.9	1
Oct-13-D	Oct-13-2015	8:26	17:48	NW-W	Sunny	11	13.84	22.4	23.7	22	3.7	1
Oct-13-N	Oct-13-2015	17:53	6:23	SW-SE	Cloudy			1.3	17.2	50	3.7	1
Oct-14-D	Oct-14-2015	8:17	17:47	S-E	Cloudy	4	2.99	12.4	20.1	45	3.5	2
Oct-14-N	Oct-14-2015	17:53	6:23	SW-NW	Cloudy			1.1	16.3	64	3.5	2
Oct-15-D	Oct-15-2015	8:28	17:33	W-NW	Sunny	9	8.31	31.9	22.5	38	3.1	2
Oct-15-N	Oct-15-2015	17:39	6:09	W	Cloudy			3.3	19.7	55	3.1	2

SH is the daily solar radiation on a horizontal surface, T is 12-hour averaged temperature, RH is 12-hour averaged relative humidity, MWS is the daily (24-hour) maximum wind speed, and WS is the daily average wind speed.

Table S2. Contents of PM_{2.5}, Hg in PM_{2.5} (PM_{2.5}-Hg) and Hg isotopic composition of PM_{2.5}-

140 Hg.

Name	PM _{2.5} (µg/m ³)	Hg Con. (µg/g)	δ ²⁰² Hg (‰)	2SD	Δ ¹⁹⁹ Hg (‰)	2SD	Δ ²⁰⁰ Hg (‰)	2SD	Δ ²⁰¹ Hg (‰)	2SD
Sept-15-N	85	0.52	-0.89	0.14	0.05	0.06	0.13	0.04	-0.08	0.07
Sept-16-D	71	0.41	-0.61	0.14	0.30	0.06	0.06	0.04	0.05	0.07
Sept-16-N	88	0.44	-0.53	0.14	-0.05	0.06	0.06	0.04	-0.11	0.07
Sept-17-D	76	0.38	-0.47	0.14	0.21	0.06	0.01	0.04	0.08	0.07
Sept-17-N	94	0.47	-0.27	0.14	-0.08	0.06	0.03	0.04	-0.15	0.07
Sept-18-D	32	0.17	-0.72	0.14	0.90	0.06	0.08	0.04	0.64	0.07
Sept-18-N	43	0.31	-1.29	0.14	0.04	0.06	-0.02	0.04	-0.12	0.09
Sept-19-D	13	0.09								
Sept-19-N	52	0.29	-0.98	0.14	0.09	0.06	0.02	0.04	-0.06	0.07
Sept-20-D	63	0.61	-0.48	0.14	0.16	0.06	0.12	0.04	0.02	0.07
Sept-20-N	63	0.89	-0.59	0.14	0.01	0.06	0.04	0.04	0.06	0.07
Sept-21-D	61	0.48	-0.34	0.14	0.50	0.06	0.05	0.04	0.34	0.07
Sept-21-N	83	0.62	-0.69	0.14	0.10	0.06	0.06	0.04	0.07	0.07
Sept-22-D	95	0.53	-0.40	0.14	0.28	0.06	0.03	0.04	0.18	0.07
Sept-22-N	23	0.31	-0.83	0.14	-0.06	0.06	-0.01	0.04	-0.09	0.07
Sept-23-D	19	0.15								
Sept-23-N	39	0.54	-0.87	0.14	0.17	0.06	0.03	0.04	0.09	0.07
Sept-24-D	84	0.38	-0.25	0.14	0.02	0.06	0.11	0.04	0.03	0.07
Sept-24-N	47	0.20	-0.47	0.14	0.05	0.06	0.06	0.04	-0.11	0.07
Sept-25-D	9	0.38	-0.49	0.14	0.21	0.06	0.18	0.04	0.21	0.07
Sept-25-N	33	0.14	-0.57	0.14	0.42	0.06	0.08	0.04	0.27	0.07
Sept-26-D	24	0.20	-0.37	0.14	1.04	0.06	0.10	0.04	0.71	0.07
Sept-26-N	51	0.44	-0.64	0.18	0.30	0.06	0.09	0.04	0.17	0.07
Sept-27-D	31	0.39	-0.30	0.14	0.76	0.06	0.12	0.04	0.61	0.07
Sept-27-N	46	0.78	-0.62	0.14	0.15	0.06	0.07	0.04	0.08	0.07
Sept-28-D	34	0.32	-0.38	0.14	-0.48	0.06	0.02	0.04	-0.52	0.07
Sept-28-N	34	0.34	-0.32	0.14	-0.46	0.06	0.01	0.04	-0.45	0.07
Sept-29-D	52	0.48	0.29	0.14	0.06	0.06	0.20	0.04	0.26	0.09
Sept-29-N	13	0.36	-0.82	0.14	-0.04	0.06	0.02	0.04	-0.03	0.07
Sept-30-D	14	0.16	-0.23	0.14	-0.13	0.06	0.16	0.04	-0.14	0.07
Sept-30-N	22	0.64	-0.26	0.14	-0.04	0.06	0.08	0.04	-0.05	0.07
Oct-1-D	7	0.12								
Oct-1-N	19	0.67	-0.91	0.14	0.11	0.06	0.11	0.04	0.09	0.07
Oct-2-D	18	0.20	-0.54	0.14	0.29	0.06	0.14	0.04	0.26	0.07
Oct-2-N	31	0.59	-1.49	0.14	0.13	0.06	-0.02	0.04	0.18	0.07
Oct-3-D	19	0.26	-0.21	0.14	0.86	0.06	0.21	0.04	0.59	0.07
Oct-3-N	39	0.59	-0.95	0.14	0.18	0.06	0.07	0.04	0.20	0.07
Oct-4-D	88	0.36	-0.80	0.14	0.27	0.06	0.02	0.04	0.09	0.07
Oct-4-N	119	0.38	-0.97	0.14	-0.11	0.06	0.02	0.04	-0.16	0.07
Oct-5-D	114	0.37	-0.32	0.14	-0.53	0.06	0.09	0.04	-0.64	0.07
Oct-5-N	138	0.53	-0.69	0.14	-0.51	0.06	0.06	0.04	-0.54	0.07
Oct-6-D	156	0.39	-0.09	0.14	-0.40	0.06	0.08	0.04	-0.57	0.07
Oct-6-N	158	0.44	0.16	0.14	-0.15	0.06	0.10	0.04	-0.12	0.07
Oct-7-D	138	0.47	0.20	0.14	0.69	0.06	0.08	0.04	0.42	0.07
Oct-7-N	128	0.46	0.52	0.14	0.55	0.06	0.14	0.04	0.39	0.07
Oct-8-D	4	0.30	-0.22	0.14	0.32	0.06	0.19	0.04	0.20	0.07
Oct-8-N	16	0.24	0.55	0.14	-0.07	0.06	0.09	0.04	0.01	0.07
Oct-9-D	24	0.43	-0.47	0.14	0.04	0.06	0.07	0.04	0.12	0.07
Oct-9-N	17	0.08								
Oct-10-D	14	0.19	-0.82	0.14	0.33	0.06	0.08	0.04	0.55	0.07
Oct-10-N	8	0.26	-0.61	0.14	0.32	0.06	0.11	0.04	0.28	0.07
Oct-11-D	12	0.10								
Oct-11-N	15	0.38	-0.42	0.14	0.17	0.06	0.14	0.04	0.20	0.07
Oct-12-D	10	0.27	-0.79	0.14	0.28	0.06	0.12	0.04	0.27	0.07
Oct-12-N	26	1.22	-0.90	0.14	-0.03	0.06	0.05	0.04	-0.03	0.07
Oct-13-D	19	0.43	-0.70	0.14	0.23	0.06	0.01	0.04	0.16	0.07
Oct-13-N	60	0.89	-0.80	0.14	-0.01	0.06	0.06	0.04	-0.06	0.07
Oct-14-D	50	0.37	-0.78	0.14	0.01	0.06	-0.01	0.04	0.00	0.07
Oct-14-N	82	0.49	-1.21	0.14	-0.20	0.06	-0.02	0.04	-0.18	0.07
Oct-15-D	50	0.34	-0.60	0.14	0.57	0.06	0.08	0.04	0.52	0.07
Oct-15-N	95	0.33	-0.37	0.14	0.21	0.06	0.07	0.04	0.33	0.07

Table S3. The below results of Paired Samples T-Test and Independent Samples T-Test were obtained using the IBM SPSS Statistics Version 22. The paired samples were consecutive day and night PM_{2.5} samples, for example, Sept-16-D and Sept-16-N were paired samples.

Paired Samples Test

Day - Night	Paired Differences					t	df	Sig. (2-tailed)
	Mean	Std. Deviation	Std. Error Mean	95% Confidence Interval of the Difference				
				Lower	Upper			
PM _{2.5}	-2.06667	78.67959	14.36486	-31.44611	27.31278	-0.144	29	0.887
Hg Con.	-0.15263	0.27183	0.04963	-0.25414	-0.05113	-3.075	29	0.005
δ ²⁰² Hg	0.16960	0.41413	0.08283	-0.00134	0.34054	2.048	24	0.052
Δ ¹⁹⁹ Hg	0.24400	0.28384	0.05677	0.12684	0.36116	4.298	24	0.000
Δ ²⁰⁰ Hg	0.04120	0.06412	0.01282	0.01473	0.06767	3.213	24	0.004

145

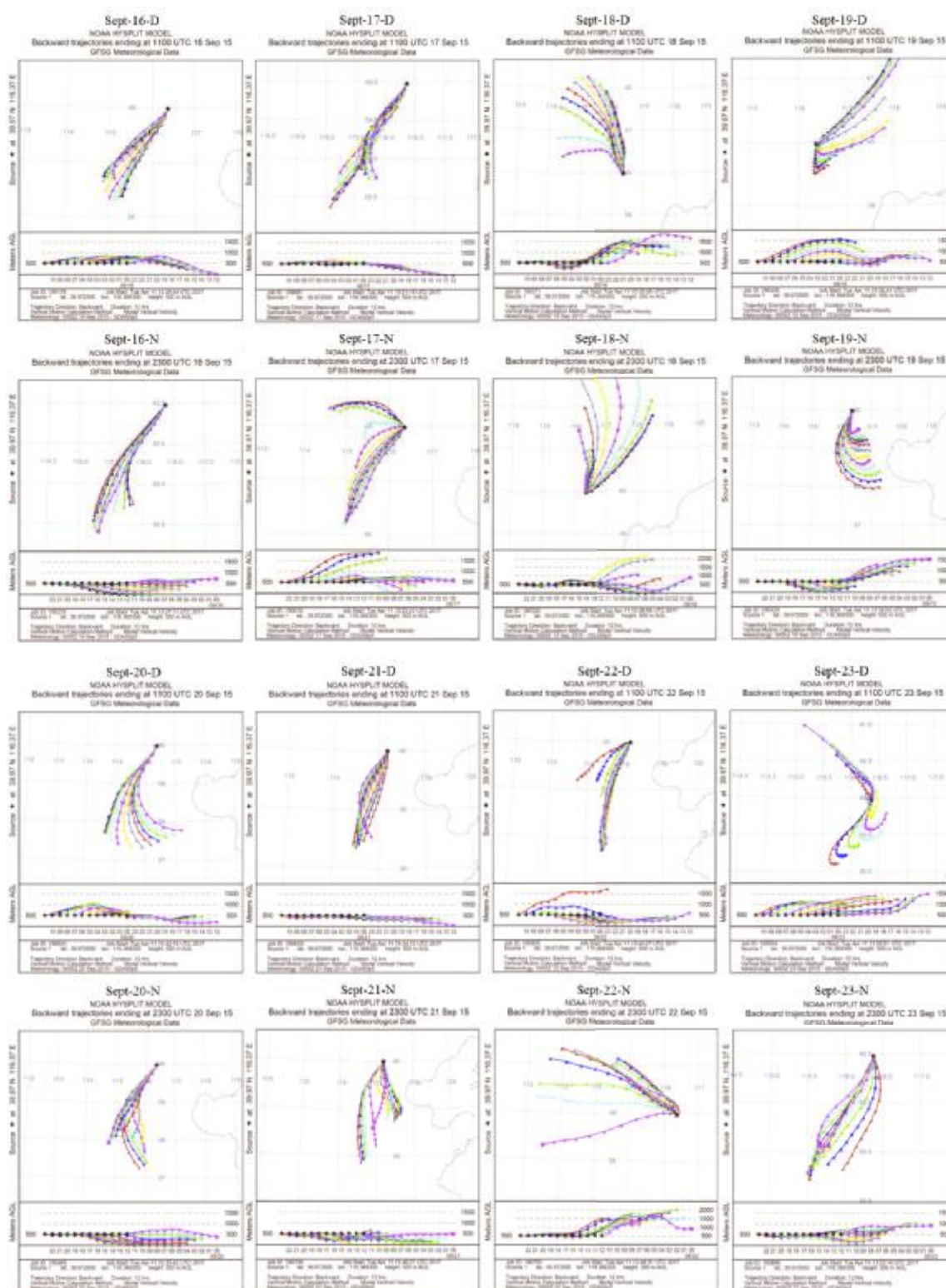
Independent Samples Test

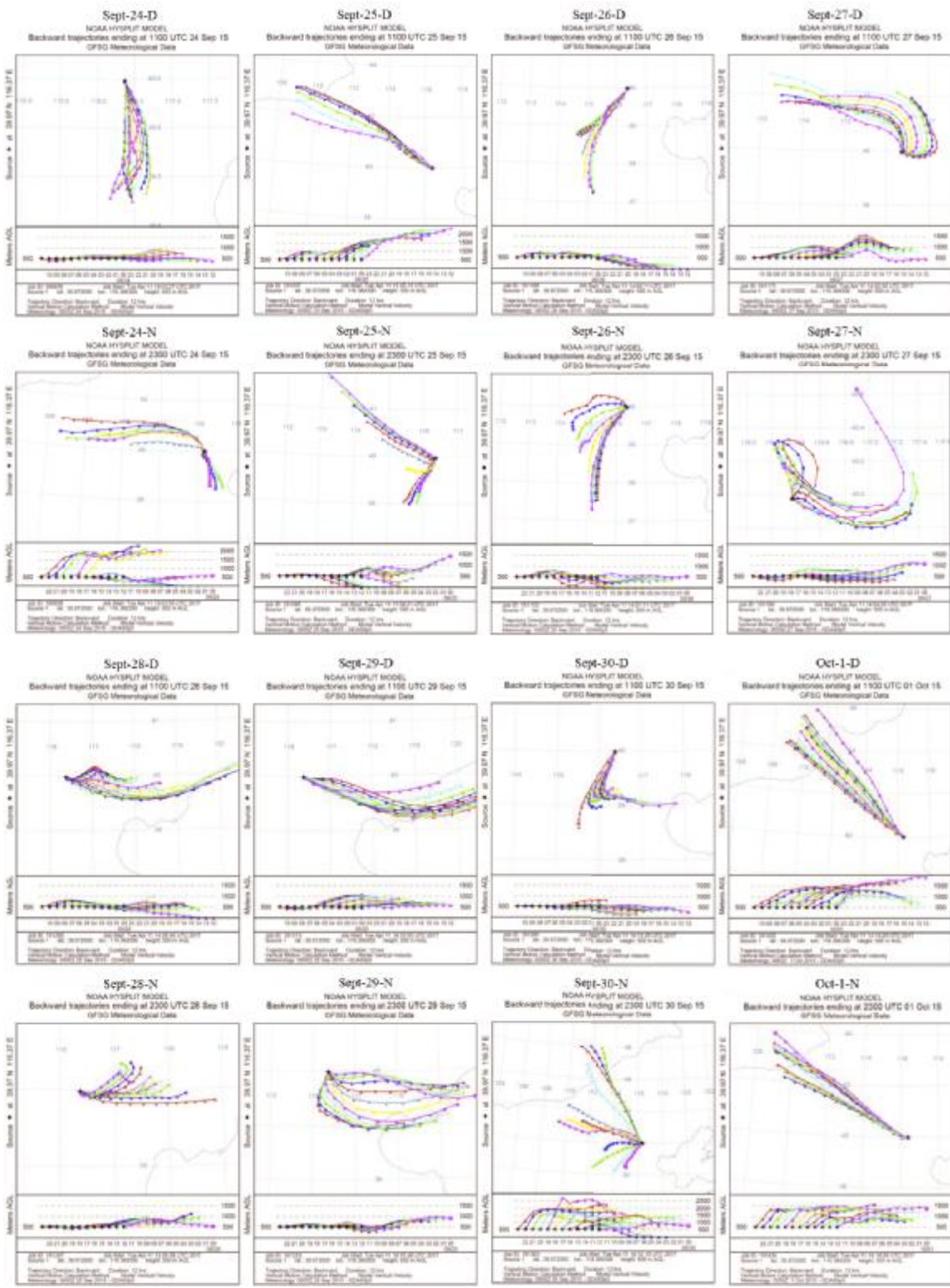
Day vs Night	Mean Difference	Std. Error Difference	95% Confidence Interval of the Difference		t	df	Sig. (2-tailed)
			Lower	Upper			
PM _{2.5}	-2.57742	22.46315	-47.52607	42.37123	-0.115	59	0.909
Hg Con.	-0.15408	0.04966	-0.25393	-0.05423	-3.103	47.858	0.003
δ ²⁰² Hg	0.20549	0.10385	-0.00272	0.41370	1.979	54	0.053
Δ ¹⁹⁹ Hg	0.21982	0.08777	0.04209	0.39755	2.505	37.666	0.017
Δ ²⁰⁰ Hg	0.03464	0.01437	0.00582	0.06346	2.410	54	0.019

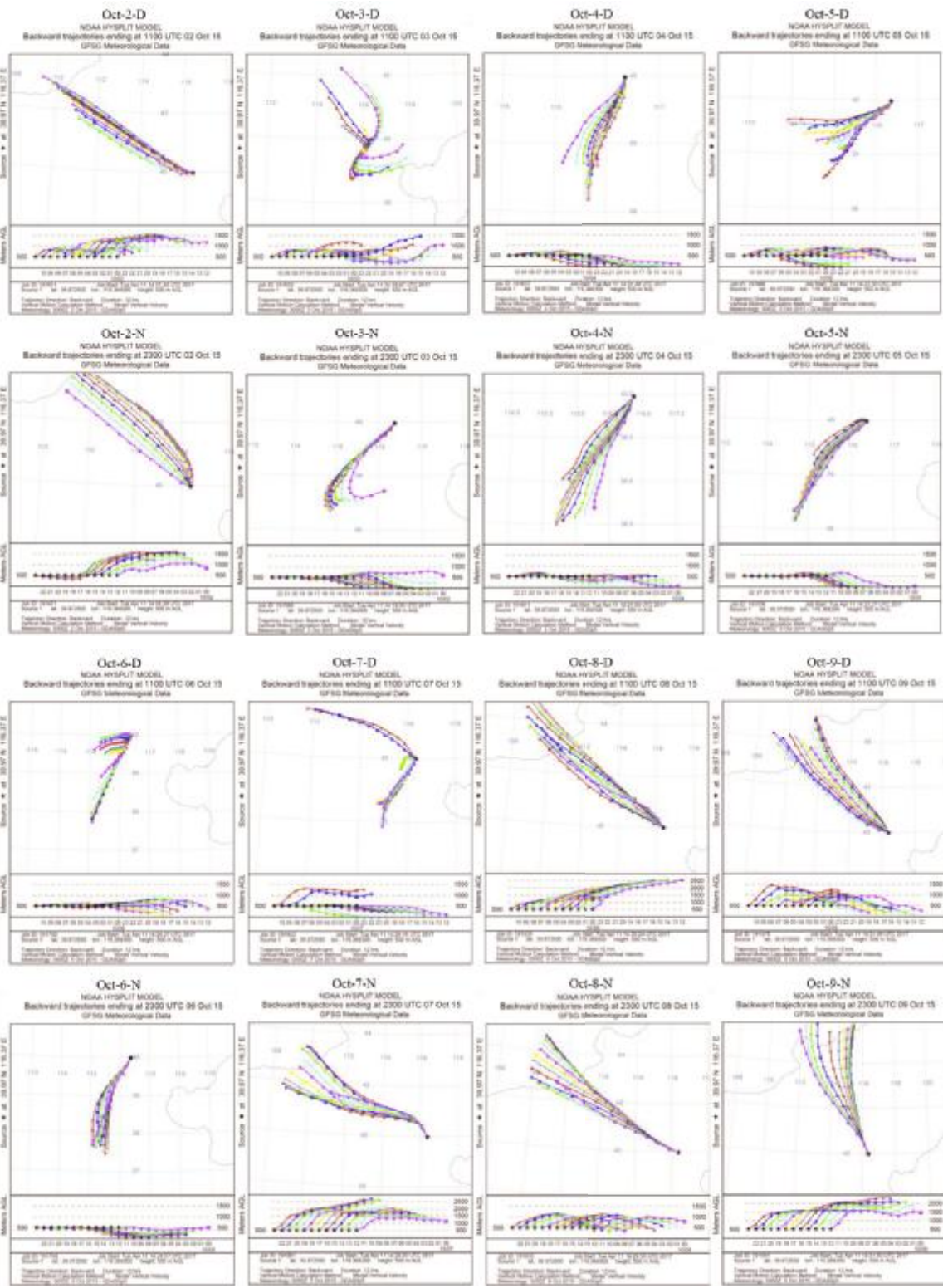
Table S4. Calculated GOM concentrations of day and night samples. The value of GOM concentrations higher at night than the consecutively days are in bold text.

Daytime samples	Ave. T (°C)	Hg Con. ($\mu\text{g g}^{-1}$)	K ($\text{m}^3 \mu\text{g}^{-1}$)	GOM (pg m^{-3})	Nighttime samples	Ave. T (°C)	Hg Con. ($\mu\text{g g}^{-1}$)	K ($\text{m}^3 \mu\text{g}^{-1}$)	GOM (pg m^{-3})
Sept-16-D	24.1	0.41	0.026	16	Sept-15-N	19.8	0.52	0.035	15
Sept-17-D	24.8	0.38	0.025	15	Sept-16-N	21.1	0.44	0.032	14
Sept-18-D	27.3	0.17	0.021	8.0	Sept-17-N	22.6	0.47	0.029	16
Sept-19-D	26.1	0.09	0.023	3.9	Sept-18-N	21.7	0.31	0.030	10
Sept-20-D	24.5	0.61	0.025	24	Sept-19-N	21.7	0.29	0.030	10
Sept-21-D	25.2	0.48	0.024	20	Sept-20-N	21.9	0.89	0.030	30
Sept-22-D	22.9	0.53	0.028	19	Sept-21-N	22.6	0.62	0.029	22
Sept-23-D	23.9	0.15	0.026	5.7	Sept-22-N	18.3	0.31	0.038	8.1
Sept-24-D	23	0.38	0.028	14	Sept-23-N	21.6	0.54	0.031	18
Sept-25-D	24.4	0.38	0.025	15	Sept-24-N	17.7	0.2	0.040	5.0
Sept-26-D	23.7	0.2	0.027	7.5	Sept-25-N	17.3	0.14	0.041	3.4
Sept-27-D	23.8	0.39	0.026	15	Sept-26-N	20.5	0.44	0.033	13
Sept-28-D	18.1	0.32	0.039	8	Sept-27-N	-	0.78		
Sept-29-D	15.7	0.48	0.046	11	Sept-28-N	17.4	0.34	0.041	8.4
Sept-30-D	18.1	0.16	0.039	4.1	Sept-29-N	14.7	0.36	0.049	7.4
Oct-1-D	19.4	0.12	0.035	3.4	Sept-30-N	15.5	0.64	0.046	14
Oct-2-D	24.3	0.2	0.026	7.8	Oct-1-N	15.8	0.67	0.045	15
Oct-3-D	22.5	0.26	0.029	9.0	Oct-2-N	18.4	0.59	0.038	16
Oct-4-D	21.5	0.36	0.031	12	Oct-3-N	17.7	0.59	0.040	15
Oct-5-D	21.8	0.37	0.030	12	Oct-4-N	17.9	0.38	0.039	10
Oct-6-D	23	0.39	0.028	14	Oct-5-N	18.3	0.53	0.038	14
Oct-7-D	22.6	0.47	0.029	16	Oct-6-N	19.8	0.44	0.035	13
Oct-8-D	17.8	0.3	0.040	7.6	Oct-7-N	19.1	0.46	0.036	13
Oct-9-D	18.7	0.43	0.037	12	Oct-8-N	14.3	0.24	0.050	4.8
Oct-10-D	14.4	0.19	0.050	3.8	Oct-9-N	12.5	0.08	0.057	1.4
Oct-11-D	20.1	0.1	0.034	3.0	Oct-10-N	15.3	0.26	0.047	5.5
Oct-12-D	22.5	0.27	0.029	9.4	Oct-11-N	16.6	0.38	0.043	8.9
Oct-13-D	23.7	0.43	0.027	16	Oct-12-N	17.8	1.22	0.040	31
Oct-14-D	20.1	0.37	0.034	11	Oct-13-N	17.2	0.89	0.041	22
Oct-15-D	22.5	0.34	0.029	12	Oct-14-N	16.3	0.49	0.044	11
					Oct-15-N	19.7	0.33	0.035	9.5

Figure S1. NOAA-HYSPLIT model shown back trajectories for 30 day-night $PM_{2.5}$ sample pairs collected during Sep. 16th to Oct. 15th 2015 from urban center of Beijing, China. Arriving air masses of 500 m above ground level (AGL) were calculated on website of <http://ready.arl.noaa.gov/hypub-bin/trajtype.pl?runtype=archive>.







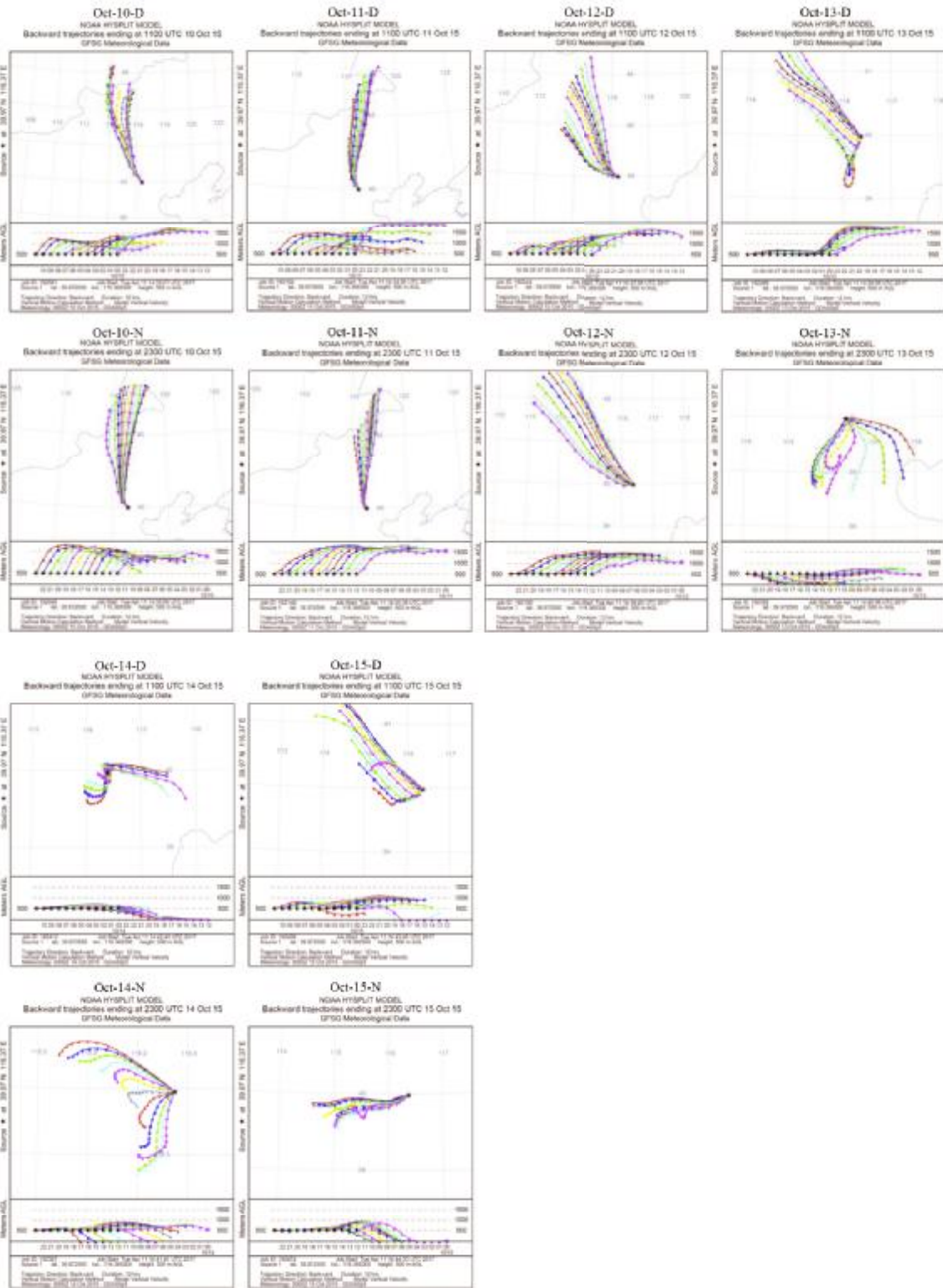
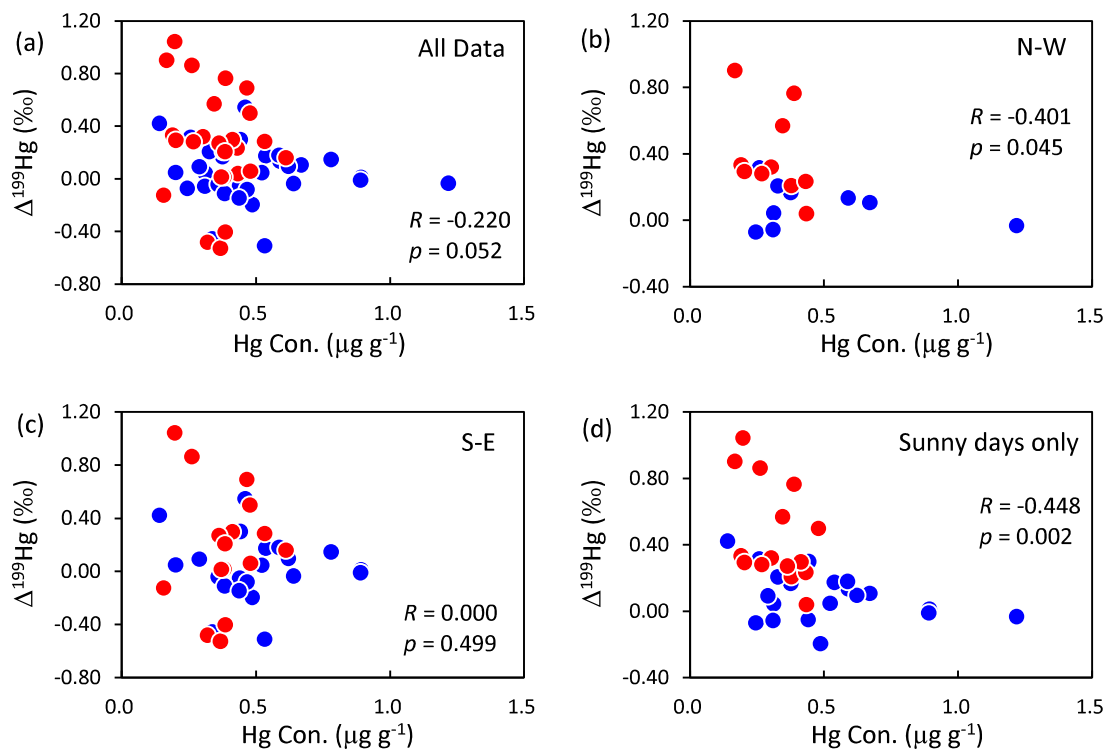
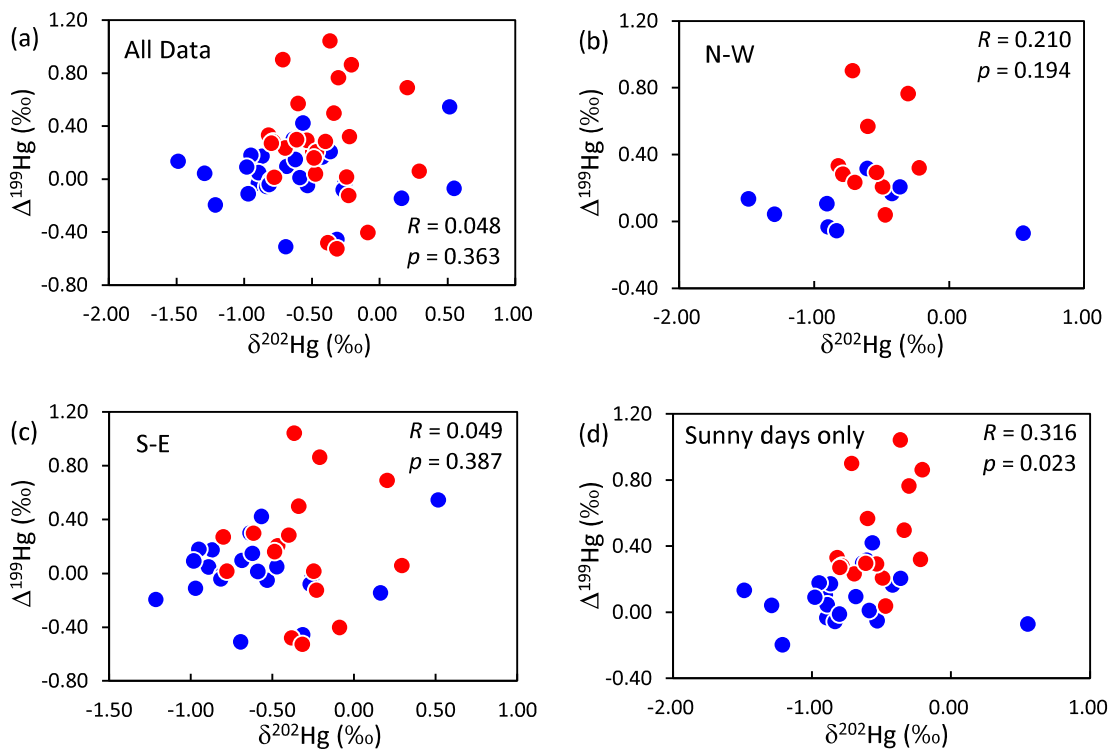


Figure S2. $\Delta^{199}\text{Hg}$ (‰) versus the content of Hg in $\text{PM}_{2.5}$ ($\mu\text{g g}^{-1}$) for different subsets of $\text{PM}_{2.5}$ samples: a) all data, b) North-West (N-W), c) South-East (S-E) and d) All sunny days (Sun), with Spearman Correlation Coefficient (R) and 1-tailed significant (p). The red circles are for daytime samples, while blue circles are for night samples.

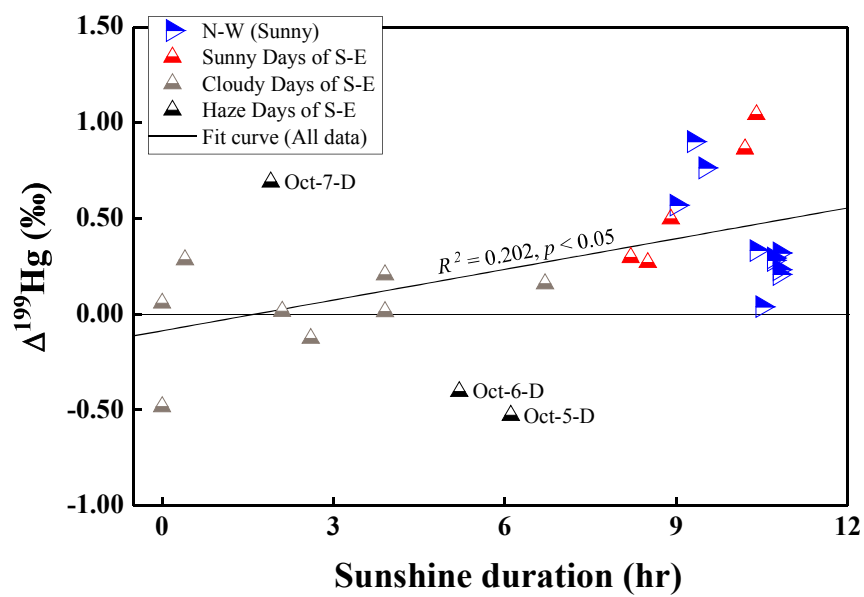


170 **Figure S3.** $\Delta^{199}\text{Hg}$ (‰) versus $\delta^{202}\text{Hg}$ (‰) for different subsets of $\text{PM}_{2.5}$ samples: a) all data, b) North-West (N-W), c) South-East (S-E) and d) All sunny days (Sun), with Spearman Correlation Coefficient (R) and 1-tailed significant (p). The red circles are for daytime samples, while the blue circles are for night samples.



175

Figure S4. $\Delta^{199}\text{Hg}$ values of daytime $\text{PM}_{2.5}$ samples versus sunshine duration (hr).



180 **Figure S5.** $\Delta^{199}\text{Hg}$ values of daytime $\text{PM}_{2.5}$ samples versus atmospheric ozone content (ppbv).

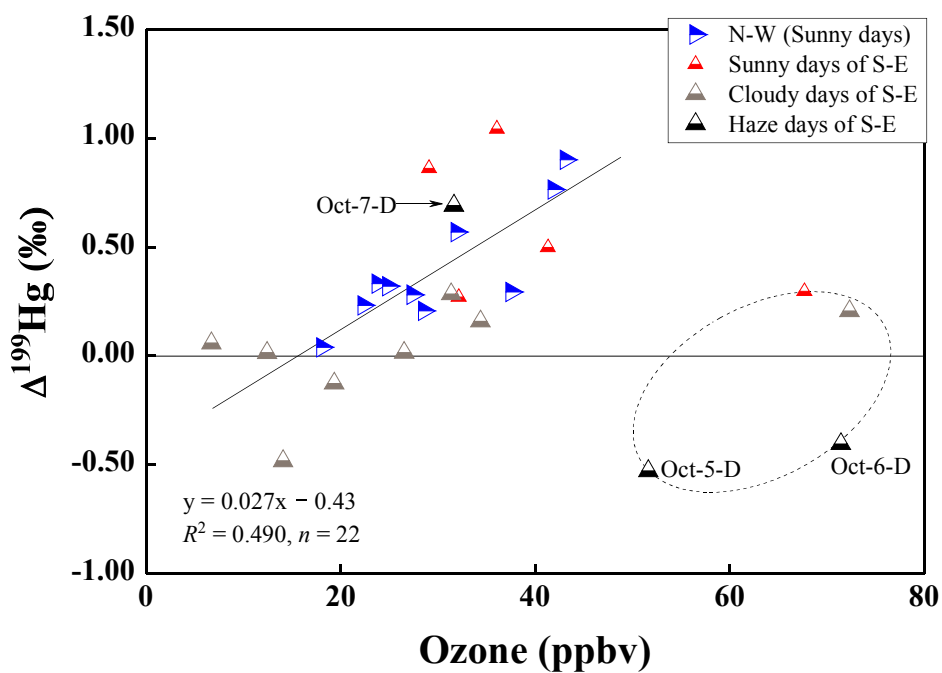


Figure S6. $\Delta^{199}\text{Hg}$ (‰) versus $\Delta^{200}\text{Hg}$ (‰) for different subsets of $\text{PM}_{2.5}$ samples: a) all data, b) North-West (N-W), c) South-East (S-E) and d) All sunny days (Sun). The red circles are for daytime samples, while the blue circles are for night samples. Positive correlations between $\Delta^{199}\text{Hg}$ and $\Delta^{200}\text{Hg}$ can be seen in each subsets, with Spearman Correlation Coefficient (R) and 1-tailed significant (p).

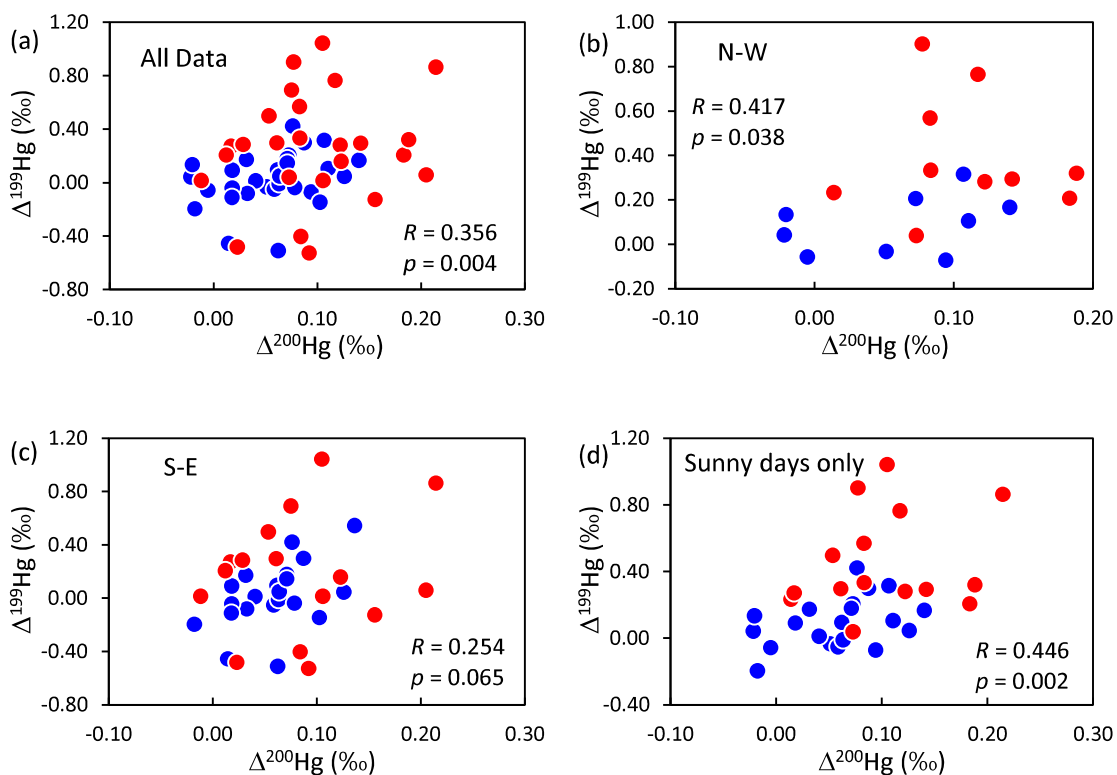
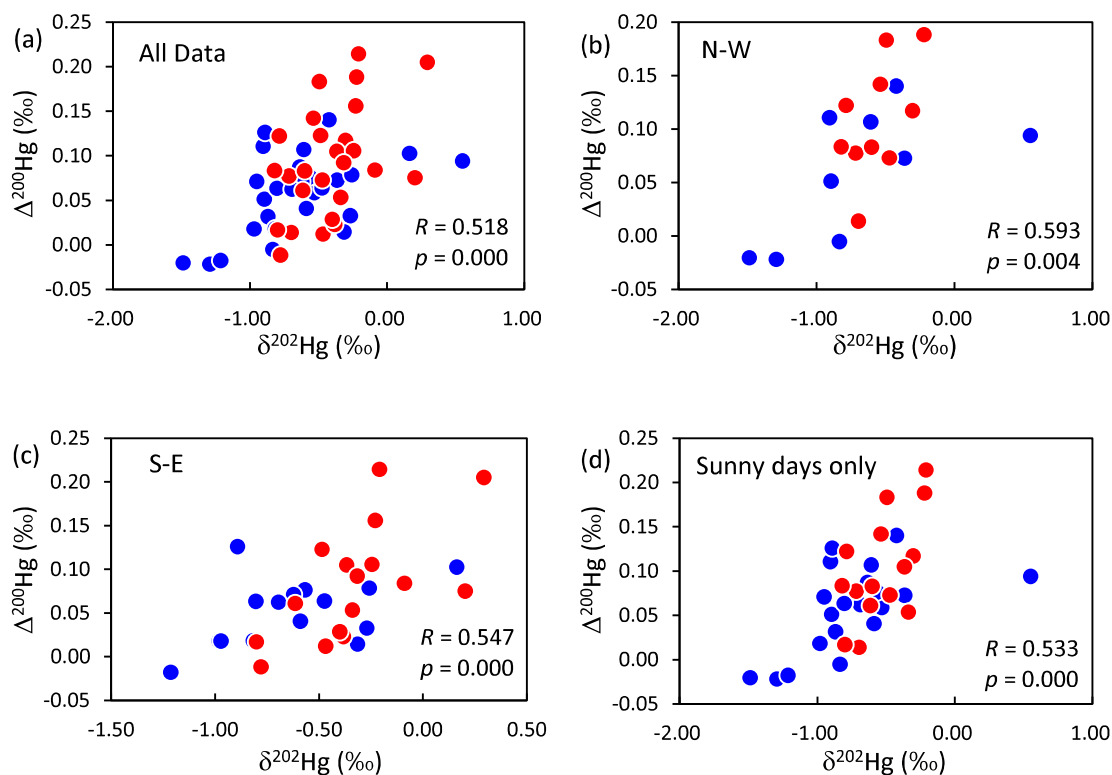


Figure S7. $\Delta^{200}\text{Hg}$ (‰) versus $\delta^{202}\text{Hg}$ (‰) for different subsets of $\text{PM}_{2.5}$ samples: a) all data, b) North-West (N-W), c) South-East (S-E) and d) All sunny days (Sun). The red circles are for daytime samples, while the blue circles are for night samples. Positive correlations between $\Delta^{200}\text{Hg}$ and $\delta^{202}\text{Hg}$ can be seen in each subsets with Spearman Correlation Coefficient (R) and

195 1-tailed significant (p).



REFERENCES

- 200 Amos, H. M., Jacob, D. J., Holmes, C. D., Fisher, J. A., Wang, Q., Yantosca, R. M., Corbitt, E. S., Galarneau, E., Rutter, A. P., Gustin, M. S., Steffen, A., Schauer, J. J., Graydon, J. A., St Louis, V. L., Talbot, R. W., Edgerton, E. S., Zhang, Y., and Sunderland, E. M.: Gas-particle partitioning of atmospheric Hg(II) and its effect on global mercury deposition, *Atmos. Chem. Phys.*, 12, 591-603, 2012.
- 205 Blum, J. D., and Bergquist, B. A.: Reporting of variations in the natural isotopic composition of mercury, *Anal. Bioanal. Chem.*, 388, 353-359, 2007.
- Huang, Q., Liu, Y. L., Chen, J. B., Feng, X. B., Huang, W. L., Yuan, S. L., Cai, H. M., and Fu, X. W.: An improved dual-stage protocol to pre-concentrate mercury from airborne particles for precise isotopic measurement, *J. Anal. At. Spectrom.*, 30, 957-966, 2015.
- 210 Huang, Q., Chen, J., Huang, W., Fu, P., Guinot, B., Feng, X., Shang, L., Wang, Z., Wang, Z., Yuan, S., Cai, H., Wei, L., and Yu, B.: Isotopic composition for source identification of mercury in atmospheric fine particles, *Atmos. Chem. Phys.*, 16, 11773-11786, 2016.
- Xiang, Y., Zhang, T., Liu, J., Lv, L., Dong, Y., and Chen, Z.: Atmosphere boundary layer height and its effect on air pollutants in Beijing during winter heavy pollution, *Atmos. Res.*, 215, 305-316, <https://doi.org/10.1016/j.atmosres.2018.09.014>, 2019.
- 215